ELSEVIER

International Journal of Solids and Structures 41 (2004) 5155–5183

INTERNATIONAL JOURNAL OF SOLIDS and STRUCTURES

www.elsevier.com/locate/ijsolstr

A spectrally formulated finite element for wave propagation analysis in layered composite media

A. Chakraborty, S. Gopalakrishnan *

Department of Aerospace Engineering, Indian Institute of Science, C.V. Raman Road, Bangalore 560012, India

Received 20 October 2003; received in revised form 9 March 2004
Available online 24 April 2004

Abstract

Wave propagation in orthotropic layered composite media due to high frequency impact loading is studied using a new spectral layer element (SLE). This novel element is formulated using the method of partial wave techniques (PWT) in conjunction with linear algebraic methodology. The matrix structure of finite element (FE) formulation is retained, which substantially simplifies the modeling of multi-layered structure. The developed SLE has an exact dynamic stiffness matrix, as it uses exact solution to the governing elastodynamic equation in frequency domain as its interpolation function. Due to this, the mass distribution is modeled exactly, and as a result, the element gives exact frequency response of each layer. Hence, one element may be as large as one complete layer and as a result system size is very small compared to conventional FE system sizes. The fast-Fourier transform (FFT) and Fourier series are used for inversion to the time/space domain. The formulated element is further used to study the stress distribution in a multi-layered media. As a natural application, Lamb wave propagation in composite plate is studied for different ply-angle and time domain description is obtained. Further, advantage of the spectral formulation in impulse force identification is demonstrated.

Keywords: Wave propagation; Orthotropic layered media; Partial wave technique; Spectral finite element; Lamb wave; Force identification

1. Introduction

Layered media are encountered in various natural (soil, wood, tissue, etc.) and artificial (bi-material, fibre reinforced composite, graded materials etc.) structural systems. All these systems are prone to dynamic loads and most often, high frequency impact loads, in their lifetime. Hence, analysis for these layered systems for impact loading is important and requires critical attention because of the following reasons.

It is quite well known that layered composite structures have low impact resistance. The impact resistance depends on the ply layup, its orientation and also on the material properties of the composite layer.

* Corresponding author. Tel.: +91-803943019; fax: +91-803600134.
E-mail address: krishnan@aero.iisc.ernet.in (S. Gopalakrishnan).

0020-7683/$ - see front matter © 2004 Elsevier Ltd. All rights reserved.
doi:10.1016/j.ijsolstr.2004.03.011

For efficiently designing the composite structures for impact loading, it is necessary to know the high frequency behavior of the structure.

Analysis of structures subjected to impact load (a load of very small duration compared to the natural time periods of the system) by conventional FE analysis is difficult because of restricted computational resources. This is because, for accurate prediction, the element sizes should be of the order of the wavelength (Kuhlemeyer and Lysmer, 1973), which is very small (since the frequency is high) and thus the cost of computation becomes enormous. Added to that is the dimension of the structure, which may be very large if e.g., a soil strata. Another way of viewing this problem is: since the energy content of the load is very high, myriad modes will get excited and unless sufficient number of elements is used the higher order mode shapes will not be captured properly and hence there will be loss of accuracy. Hence, conventional time domain FE method is computationally prohibitive for such problems. This takes us to the realm of frequency domain analysis and in particular, Spectral analysis.

Spectral analysis, as outlined by Chatfield (1984), is the synthesis of waveforms from the superposition of many frequency components, has been developed as a method based on matrix methodology by Doyle (1997), which is called the spectral finite element method (SFEM). As in conventional FE method, in SFEM, the nodal displacements are related to nodal forces through a frequency dependent dynamic stiffness matrix. The matrix-vector equation is solved for each frequency and quantities of interest are transformed back to time domain through inverse fast Fourier transform. Primary works in one dimensional waveguides can be found in Doyle (1988) and Doyle and Farris (1990). Wave propagation in multiply connected one dimensional higher order isotropic wave guides was studied by Gopalakrishnan et al. (1992) and Martin et al. (1994). In the area of composites, the SFEM is used to develop Euler–Bernoulli beam (Roy Mahapatra et al., 2000) and Timoshenko beam (Roy Mahapatra and Gopalakrishnan, 2003a), beam with embedded delamination (Nag et al., 2003) and composite tubes (Roy Mahapatra and Gopalakrishnan, 2003b).

Spectral element (SE) for 2D model is formulated by following the same procedures as in 1D case, where interfacial displacements are related to interfacial tractions through frequency dependent stiffness matrix. However, the stiffness needs to be established in frequency and wavenumber domain, where the later can be thought of as spatial frequency. Contribution from distributed mass can be represented exactly and consequently, elements need not to be small, and they can extend from one interface to another. Spectral element for isotropic layered solids was formulated by Rizzi (1989) and Rizzi and Doyle (1989, 1991). Further, 2D isotropic plates and shells were analyzed by Doyle (1997). A spectral element for inhomogeneous layered media was developed Chakraborty and Gopalakrishnan (2003), where an approximate spectrum relation was established.

There are few other works where wave propagation in layered media was treated in a slightly different way. A matrix formulation for the propagation of plane elastic waves through a stratified medium was first developed by Thomson (1950) and Haskell (1953). It relates the displacements and loads at one interface to those at another through a propagator matrix. Further development of the method, including the ability to handle generally crested waves and a discrete form of the inversion procedures, are summarized by Kennett (1983).

The limitations of the SLE formulation of Rizzi and Doyle (1991), is that Helmhöltz decomposition of the displacement field in terms of a scalar and vector potential is required, apriori. There is an advantage in the decomposition. It uncouples the governing Navier's equation and generates two Helmhöltz equations in terms of scalar and vector potential, which are solvable readily. Solution for the displacement field is then obtained from these two exact solutions and the element is formulated. But for anisotropic materials and other structural approximations like plates and shells, finding the potential itself is a difficult task and even if it is found, they may not uncouple the governing equations (Rose, 1999). Hence, the formulation must be carried out without any knowledge of the potentials. There is another important distinction between isotropic and anisotropic media. In isotropic materials, only pure modes (longitudinal and shear) are possible,

i.e., polarization vector is either parallel or normal to the propagation direction. However, for anisotropic media, pure modes can occur for some propagation directions depending upon the degree of symmetry of the material under consideration (Nayfeh, 1995). Another definition of pure modes given by Solie and Auld (1973) states that when propagation direction coincides with the direction of energy flow, the modes of propagation are pure modes. This kind of wave also occurs in anisotropic material only under certain material symmetry condition. For this reason, the waves in anisotropic materials are named quasi-longitudinal (QP) wave and quasi-shear waves (QSH and QSV), to differentiate from their isotropic counterparts. The most exhaustive treatment of wave propagation in layered composite media is given by Nayfeh (1995). Further discussion on this subject can be found in Rose (1999). Other than these two books, the literature on wave propagation in laminates due to low-velocity impact is limited in numbers, mostly studied by Mal and Lih (1992) and Lih and Mal (1992, 1995, 1996) and Mal (2002). Further, wave propagation in composite laminate for anti-plane loading was studied by Ma and Huang (1995), where closed form expressions were found for displacements and stresses.

The most general method of treating the propagation of elastic waves in anisotropic media is the partial wave technique (PWT) (Solie and Auld, 1973). The essence of the technique is to satisfy the governing equation and the appropriate boundary conditions by taking a superposition of two upward traveling plane wave modes (i.e., one quasi-longitudinal and one quasi-shear) and two downward traveling plane wave modes. Each of the four waves (six in three dimension) is termed as partial wave because they all combine to give a single guided wave mode of the layer. As the partial waves satisfy the governing equation individually, any linear combination of these waves also satisfy the governing equation (since the equation is homogeneous). The coefficients of this waves must be chosen to ensure that the appropriate boundary conditions are satisfied at the upper and lower surface of the layer.

So far, we see that all the works on the development of the SE for composite material are confined to 1D structures and no element exists for the analysis of wave propagation in composite layered media. In this work, a SE is formulated for general anisotropic layer, where, in the element formulation, we propose a simplified way of finding the wavenumbers and wave amplitudes numerically, which together construct the partial waves. As all the four wavenumbers are computed at a time, as opposed to the other methods (Roy Mahapatra et al., 2000; Roy Mahapatra and Gopalakrishnan, 2003a,b), there is no way to identify the different modes. While deriving the stiffness matrix it is an added advantage if the modes can be identified. However, in the present formulation, the knowledge of the modes is not essential. Once the partial waves are found, the wave coefficients are obtained for general stressed boundary conditions, i.e., two non-zero tractions are specified at the top and bottom of the layer. Here, it differs from other formulation based on the PWT, as no specific problem oriented boundary conditions are imposed. Thus a system matrix is established, which relates the tractions at the interface to interfacial displacements. This generalization enables the use of the system matrix as a finite element dynamic stiffness matrix, although formulated in frequency/wavenumber domain. These matrices can be assembled to model different layer of different ply-orientation, which obviates the necessity of cumbersome computation associated with multi-layer analysis, (e.g., Rose, 1999). The advantage of the present formulation in association with the PWT is in its application to construct element stiffness matrix for a wide range of structures (like plates and shells) and materials (inhomogeneous and viscoelastic). In particular viscoelastic layers can be analyzed in much more comfortable way compared to FE analysis, as the whole formulation is done in frequency domain. However, in the present manuscript, we have restricted ourselves to elastic anisotropic materials.

Another advantage of the present formulation is the ease in capturing the Lamb wave (Viktorov, 1967) propagation in anisotropic plate. By definition the Lamb waves are guided waves propagating in a domain bounded by two parallel traction-free surfaces. The importance of Lamb waves in NDE applications lies in its ability to inspect large areas at a time by propagating long distance without attenuation. Hence, they find immense application in structural health monitoring. Historically, dispersion relation (phase velocity–frequency relation) for anisotropic materials was given first by Solie and Auld (1973), where partial wave

techniques were used. However, the relation was obtained for a (0 0 1)-cut copper plate. Subsequent investigations on modeling aspects of Lamb waves were carried out by several researchers (Nayfeh, 1995). Finite Element modeling of Lamb waves was performed by Verdict et al. (1996). On the basis of discrete layer theory and multiple integral transform an analytical-numerical approach is given by Veidt et al. (2002). A coupled FE-normal mode expansion method is given by Moulin et al. (2000). Similarly Boundary Element-normal mode expansion method is given by Zhao and Rose (2003). The present formulation by virtue of frequency-wavenumber domain representation of solution is an inexpensive way of constructing the Lamb wave modes as well as predicting time domain signals.

Another important issue related to composite material is solving inverse problems, in particular, material and force identification. To the best of authors' knowledge, there are very few works reported on force reconstruction in composite structures. The present element is suitable for force identification because the frequency response function (FRF) of the modeled system, is a direct by-product of the SE procedure. The convenience and versatility of SE in conjunction with experimental data was demonstrated earlier to predict force history in mono-material beam (Doyle, 1984), bi-material beam (Doyle, 1993), isotropic plates (Doyle, 1987a), orthotropic plates (Doyle, 1987b), isotropic layered media (Rizzi and Doyle, 1991) and inhomogeneous layered media (Chakraborty and Gopalakrishnan, 2003, submitted).

There are many instances, where cost of a prototype or difficulty in obtaining a suitable physical model for impact testing preclude any experimental evaluation and numerical simulation becomes the only option for parameter estimation. Also, several difficulties are associated with wave propagation experiments performed over a finite length models in terms of noises and boundary reflections. For accurate force prediction, complete trace of the measured signal is required. The experimentally generated signal required to be truncated at some point. Choosing the point of truncation requires critical consideration since valuable information may be lost in pre-mature truncation. For dispersive system, in particular, caution should be exercised in selection of this truncation points, as the wave response will not die down completely within the chosen time window. In earlier works on inhomogeneous plate (Chakraborty and Gopalakrishnan, 2003, submitted), FE responses were taken as surrogate experimental results. Since experimental outputs are always truncated at some point depending upon the constraints of the set-up, data acquisition system and other facilities, the FE response should be taken such that it simulates closely the experimental results. When this truncated response is given as input to the SE solver, the force data can be reconstructed by performing inverse analysis. The same idea is used in this work to identify the applied impact force from the FE responses.

The manuscript is organised as follows. In Section 2, detail of the SLE formulation is given. In Section 3, several numerical examples are discussed. First, the efficiency and accuracy of the present element is demonstrated. Next, stress waves in layered media is investigated. Next, Lamb waves in anisotropic layered media are captured. Finally, applied impact force is reconstructed from FE signal. In Section 4, conclusions are drawn.

2. Spectral layer element formulation

It is assumed that there is no heat conduction in and out of the system, displacements are small, material is homogeneous and anisotropic and the domain is in two dimensional (2D) Euclidean space. The general elastodynamic equation of motion for three dimension is given by

$$\sigma_{ij,j} = \rho \ddot{u}_i, \quad \sigma_{ij} = C_{ijkl}\epsilon_{kl}, \quad \epsilon_{ij} = (u_{i,j} + u_{j,i})/2. \tag{1}$$

For 2D model with orthotropic material construction, complexity of the above equation can be further reduced by the following assumptions. The non-zero displacements are $u_1 = u$ and $u_3 = w$ in the direction $x_1 = x$ and $x_3 = z$, respectively. The non-zero strains are related to these displacements by

$$\epsilon_{xx} = u_x, \quad \epsilon_{zz} = w_z, \quad \epsilon_{xz} = u_z + w_x. \tag{2}$$

The non-zero stresses are related to these strains by the relation

$$\sigma_{xx} = Q_{11}\epsilon_{xx} + Q_{13}\epsilon_{zz}, \quad \sigma_{zz} = Q_{13}\epsilon_{xx} + Q_{33}\epsilon_{zz}, \quad \sigma_{xz} = Q_{55}\epsilon_{xz}, \tag{3}$$

where Q_{ij}s are the stiffness coefficients, which depend on the ply layup and its orientation. The expressions of Q_{ij}s are given in Reddy (1996). Substituting these stresses in the governing equation the elastodynamic equation for 2D orthotropic media is

$$\begin{aligned} &Q_{11}u_{xx} + (Q_{13} + Q_{55})w_{xz} + Q_{55}u_{zz} = \rho\ddot{u}, \\ &Q_{55}w_{xx} + (Q_{13} + Q_{55})u_{xz} + Q_{33}w_{zz} = \rho\ddot{w}. \end{aligned} \tag{4}$$

The displacement field is assumed to be a synthesis of frequency and wavenumbers, both horizontal and vertical, as

$$u(x,z,t) = \sum_{n=1}^{N-1}\sum_{m=1}^{M-1} \hat{u}(z,\eta_m,\omega_n)\begin{Bmatrix} \sin(\eta_m x) \\ \cos(\eta_m x) \end{Bmatrix} e^{j\omega_n t}, \tag{5}$$

$$w(x,z,t) = \sum_{n=1}^{N-1}\sum_{m=1}^{M-1} \hat{w}(z,\eta_m,\omega_n)\begin{Bmatrix} \cos(\eta_m x) \\ \sin(\eta_m x) \end{Bmatrix} e^{j\omega_n t}, \tag{6}$$

where ω_n is the discrete angular frequency, η_m is the discrete horizontal wavenumber and $j^2 = -1$. The X dependency of the displacement field (sine or cosine) will be determined based upon the loading pattern. For loads having symmetric distribution about Z axis, *sine* function for u and *cosine* function for w are to be chosen. In all subsequent formulation and computation, symmetric load pattern will be considered. Discrete values of η_m depend upon the X window length and number of mode shapes (M) chosen. In what follows, boldface uppercase and lowercase letters denote matrices and vectors, respectively.

To get the expression for $\hat{u}(z)$ and $\hat{w}(z)$, Eqs. (5) and (6) need to be substituted in Eq. (4), which results in two ordinary differential equations (ODEs) for $\hat{u}(z)$ and $\hat{w}(z)$ in which ω_n and η_m will be present as parameters. The equation in matrix vector notation is

$$\mathbf{A}\hat{\mathbf{u}}'' + \mathbf{B}\hat{\mathbf{u}}' + \mathbf{C}\hat{\mathbf{u}} = \mathbf{0}, \quad \hat{\mathbf{u}} = \{\hat{u} \ \ \hat{w}\}, \tag{7}$$

where prime denotes differentiation with respect to z. The matrices $\mathbf{A}$, $\mathbf{B}$ and $\mathbf{C}$ are

$$\mathbf{A} = \begin{bmatrix} Q_{55} & 0 \\ 0 & Q_{33} \end{bmatrix}, \quad \mathbf{B} = \begin{bmatrix} 0 & -(Q_{13} + Q_{55})\eta_m \\ (Q_{13} + Q_{55})\eta_m & 0 \end{bmatrix}, \tag{8}$$

$$\mathbf{C} = \begin{bmatrix} -\eta_m^2 Q_{11} + \rho\omega_n^2 & 0 \\ 0 & -\eta_m^2 Q_{55} + \rho\omega_n^2 \end{bmatrix}. \tag{9}$$

For homogeneous material these ODEs are of constant coefficients and solutions are in the form of $u_0 e^{-jkz}$ and $w_0 e^{-jkz}$ where u_0, w_0 and k, the vertical (Z direction) wavenumbers, are unknowns. Substituting these solutions in Eq. (7), the problem becomes of finding non-trivial u_0, w_0 from the equation

$$\mathbf{W}\{\mathbf{u}_0\} = \mathbf{0}, \quad \mathbf{W} = -k^2\mathbf{A} - jk\mathbf{B} + \mathbf{C}, \quad \{\mathbf{u}_0\} = \{u_0 \ w_0\}, \tag{10}$$

where $\mathbf{W}$ is called the wave matrix. As we are interested in non-trivial values of $\mathbf{u}_0$, the wave matrix must be singular, i.e., determinant of the matrix must be zero, which is the required condition for finding the wavenumber k. The wave matrix in explicit form is

$$\mathbf{W} = \begin{bmatrix} -k^2 Q_{55} - \eta_m^2 Q_{11} + \rho\omega_n^2 & jk\eta_m(Q_{13} + Q_{55}) \\ -jk\eta_m(Q_{13} + Q_{55}) & -k^2 Q_{33} - \eta_m^2 Q_{55} + \rho\omega_n^2 \end{bmatrix}. \tag{11}$$

The singularity condition of **W** yields

$$Q_{33}Q_{55}k^4 + \{(Q_{11}Q_{33} - 2Q_{13}Q_{55} - Q_{13}^2)\eta_m^2 - \rho\omega_n^2(Q_{33} + Q_{55})\}k^2 + \{Q_{11}Q_{55}\eta_m^4 - \rho\omega_n^2\eta_m^2(Q_{11} + Q_{55}) + \rho^2\omega_n^4\} = 0. \tag{12}$$

The above equation which relates vertical wavenumber k to the horizontal wavenumber η and frequency ω is called the spectrum relation. It is to be noted that for each value of η_m and ω_n, there are four values of k, denoted by $k_{lmn}, l = 1, \ldots, 4$, which will be obtained by solving the spectrum relation. Explicit solution of the wavenumber k is $k_{lnm} = \pm\sqrt{-b \pm \sqrt{b^2 - 4ac}}$, where a, b and c are the coefficients of k^4, k^2 and k^0, respectively, in Eq. (12).

There are certain properties of the wavenumbers which will be explored now. As can be seen from Eq. (12), for $\eta_m = 0$, the equation is readily solvable to give the roots $\pm\omega\sqrt{\rho/Q_{33}}$ and $\pm\omega\sqrt{\rho/Q_{55}}$. Since, none of the ρ, Q_{33} or Q_{55} can be negative or zero, these roots are always real and linear with ω. When η_m is not zero, k becomes zero for ω satisfying

$$\begin{aligned} &Q_{11}Q_{55}\eta_m^4 - \rho\omega_n^2\eta_m^2(Q_{11} + Q_{55}) + \rho^2\omega_n^4 = 0, \\ &\text{i.e., } (Q_{11}\eta_m^2 - \rho\omega^2)(Q_{55}\eta_m^2 - \rho\omega^2) = 0, \\ &\text{i.e., } \omega = \eta_m\sqrt{Q_{11}/\rho}, \quad \eta_m\sqrt{Q_{55}/\rho}. \end{aligned} \tag{13}$$

Before these frequencies, the roots are imaginary and non-propagating and after these frequencies, the roots are real and propagating. These frequencies are called cut-off frequencies. For isotropic materials they are given by $c_p\eta$ and $c_s\eta$ (Rizzi, 1989). The current expressions for cut-off frequencies are also reducible to that of isotropic materials if we identify Q_{11} and Q_{55} with $\lambda + 2\mu$ and μ, respectively, where λ and μ are the Lame's parameters. If we identify QP wave with Q_{33} (or Q_{11}) and QSV wave with Q_{55}, then as the cut-off frequencies suggest, for the same value of η_m, it is the QSV wave that becomes propagating first, since $Q_{11} > Q_{55}$. The wavenumbers of positive roots denote forward propagating modes and the negative roots denote backward propagating modes. In Fig. 1, the wavenumbers are plotted for three different ply-angles, 0°, 45° and 90°. For all the ply-angles, Q_{33} and Q_{55} are assumed 9.69 GPa and 4.13 GPa, respectively. For

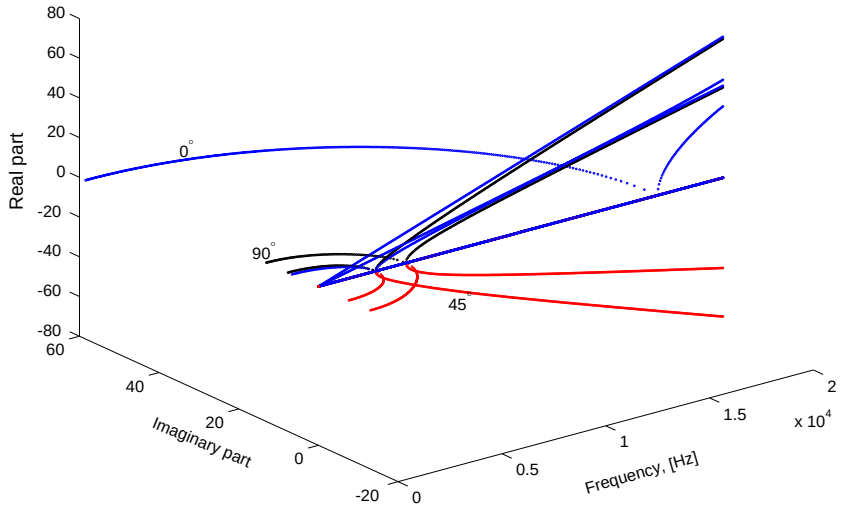

Fig. 1. Variation of wavenumber with ω_n ($\eta_m = 10$).

Q_{11} and Q_{13}, following values are assumed. For 0°, $Q_{11} = 146.3$ GPa and $Q_{13} = 2.98$ GPa, for 45°, $Q_{11} = 44.62$ GPa and $Q_{13} = 1.62$ GPa and for 90°, $Q_{11} = 9.69$ GPa and $Q_{13} = 2.54$ GPa. In Fig. 1, imaginary part of the wavenumbers is plotted in horizontal plane and real part in the vertical plane. Further, the imaginary part of the wavenumbers for 0° and 90° are plotted in the positive side, whereas for 45° it is plotted in the negative side, for distinction. Two different η_m values are taken. The linear variation of the real part of the wavenumbers are for $\eta_m = 0$ and rest of the plots are for $\eta_m = 10$. As discussed previously, slope of the linear portion depends upon Q_{33} and Q_{55} and as they are equal for all the ply-angles, this part is common for all the ply-angles. The difference comes in the imaginary part and cut-off frequencies. Two different cut-off frequencies are seen in the figure for each ply-angle, where the largest value is for 0° ply-angle because of its largest Q_{11}. Further, the shear cut-off frequency is same for all the ply-angles as Q_{55} is equal in all the cases.

Once, the required wavenumbers k are obtained, for which the wave matrix $\mathbf{W}$ is singular, we can evaluate $\mathbf{u}_0$ through the solution of

$$\begin{Bmatrix} u_0 \\ w_0 \end{Bmatrix} = \sum_{n=1}^{4} \begin{Bmatrix} A_n \\ B_n \end{Bmatrix} \mathrm{e}^{-\mathrm{j}k_n z}. \tag{14}$$

Above expression involves a total of 8 constants. However, they are inter-dependent and only four independent constants exist. This can be seen by substituting the solution in Eq. (10), which yields $W_{11}A_n + W_{12}B_n = 0$, or, $W_{21}A_n + W_{22}B_n = 0$. Since, for the solved values of the wavenumber k, the wave matrix is singular, these two conditions are not linearly independent, and anyone of the two conditions can be used to express one of the constants in terms of the another. However, in doing so, it should be known apriori, which elements of the wave matrix are not zero. Only those elements can be used as denominators while establishing the relation. This approach is followed in more recent works (Roy Mahapatra et al., 2000; Roy Mahapatra and Gopalakrishnan, 2003a,b) in formulating one dimensional elements. However, for more complicated problems involving more than three variables (as to be encountered in plates and shells), the method becomes very tedious and some alternative is necessary. It is to be noted that for isotropic materials this problem does not arise at all because of the introduction of Helmhöltz decomposition.

In short, for problems with more than two independent variables, a different procedure is necessary. We propose here a formulation technique which will be a general one, applicable to any structural systems with no Helmhöltz decomposition. Here, the displacement field for the frequency ω_n and wavenumber η_m is written as

$$u_{nm} = R_{11}C_1\mathrm{e}^{-\mathrm{j}k_1 x} + R_{12}C_2\mathrm{e}^{-\mathrm{j}k_2 x} + R_{13}C_3\mathrm{e}^{+\mathrm{j}k_1 x} + R_{14}C_4\mathrm{e}^{+\mathrm{j}k_2 x}, \tag{15}$$

$$w_{nm} = R_{21}C_1\mathrm{e}^{-\mathrm{j}k_1 x} + R_{22}C_2\mathrm{e}^{-\mathrm{j}k_2 x} + R_{23}C_3\mathrm{e}^{+\mathrm{j}k_1 x} + R_{24}C_4\mathrm{e}^{+\mathrm{j}k_2 x}, \tag{16}$$

where R_{ij} are amplitude coefficients to be determined and they are called wave amplitudes. In the works of Roy Mahapatra et al. (2000) and Roy Mahapatra and Gopalakrishnan (2003a,b), the wave amplitudes are obtained by using the wave matrix $\mathbf{W}$. As outlined earlier, for isotropic material (Rizzi and Doyle, 1991), R_{ij} s are explicitly known. However, for anisotropic material they are to be computed numerically. For each wavenumber k_{inm} ($i = 1, \ldots, 4$), the ith column of the wave amplitude matrix $\mathbf{R}$, satisfy

$$[\mathbf{W}(k_{inm})] \begin{Bmatrix} R_{1i} \\ R_{2i} \end{Bmatrix}_{nm} = \begin{Bmatrix} 0 \\ 0 \end{Bmatrix}, \tag{17}$$

since none of the constants $C_i, i = 1, \ldots, 4$, is zero. Eq. (17) suggests where to look for the elements of the wave amplitude matrix. They are exactly the elements of the null space of $\mathbf{W}$. Since, $\mathbf{W}(k_{inm})$ is singular for each k_{inm}, the null space of each $\mathbf{W}(k_{inm})$ has a non-trivial element and that will serve the purpose of the ith column of $\mathbf{R}$.

To find the element of the null space of **W**, singular value decomposition (SVD) can be utilized which states that, for any rectangular matrix **A** of complex entries (Golub and Loan van, 1996), there exist unitary matrices **U** and **V** and diagonal matrix **S**, such that $\mathbf{A} = \mathbf{USV}^{\mathrm{H}}$, where $(\cdot)^{\mathrm{H}}$ denotes Hermitian conjugate. The entries of **S** are the singular values. The most important property of these unitary matrices that is useful here is that the columns of **V** that correspond to zero singular values (zero diagonal elements of **S**) are elements of basis of the null space of **A**. Since, all we need is an element of the null space we can as well take the elements of the basis itself. Utilizing this fact, SVD of **W** is performed for each value of k_{inm}, ω_n and η_m to get $\mathbf{R}_{nm}$.

Once the four wavenumbers and wave amplitudes are known, the four partial waves can be constructed and the displacement field can be written as a linear combination of the partial waves. Each partial wave is given by

$$\mathbf{a}_i = \begin{Bmatrix} u_i \\ w_i \end{Bmatrix} = \begin{Bmatrix} R_{1i} \\ R_{2i} \end{Bmatrix} \mathrm{e}^{-\mathrm{j}k_i z} \begin{Bmatrix} \sin(\eta_m x) \\ \cos(\eta_m x) \end{Bmatrix} \mathrm{e}^{\mathrm{j}\omega_n t}, \quad i = 1, \ldots, 4, \tag{18}$$

and the total solution is

$$\mathbf{u} = \sum_{i=1}^{4} C_i \mathbf{a}_i \tag{19}$$

It is evident that this method is applicable for wave matrix of any size and thus suitable for plate and shell formulation. There is another advantage of this method. If the spectrum relation is solved using companion matrix method, then it is not possible to keep track of the each individual wavenumbers and **R** matrix formulation by methods proposed by Roy Mahapatra et al. (2000) and Roy Mahapatra and Gopalakrishnan (2003a,b), fails. In the present method, there is no need to keep track of each individual wavenumber. As the element of the null space is computed numerically, rather than analytically, there is no need to check for the non-trivial elements of wave matrix.

2.1. Finite Layer Element (FLE)

Once the solutions of u and w are obtained in the form of Eqs. (15) and (16) for each value of ω_n and η_m, the shape functions required for element formulation can be formed in the following way. The solution of u_{nm} and w_{nm} (Eqs. (15) and (16)) contains four independent constants (C_i) which are to be replaced by the nodal displacements of node 1 and node 2, i.e., u_{1nm}, w_{1nm}, u_{2nm} and w_{2nm}. For that, the expressions of u_{nm} and w_{nm} are evaluated at node 1 ($z = 0$) and node 2 ($z = L$) and equated to the nodal displacements. This operation yields a relation between nodal displacements and the constants C_i as

$$\{u_{1nm} \quad v_{1nm} \quad u_{2nm} \quad v_{2nm}\}^{\mathrm{T}} = [\mathbf{T_{1nm}}] \{C_1 \quad C_2 \quad C_3 \quad C_4\}^{\mathrm{T}}, \tag{20}$$

i.e.,

$$\{\hat{\mathbf{u}}\}_{nm} = [\mathbf{T_1}]_{nm} \{\mathbf{C}\}_{nm}, \tag{21}$$

where $\{\cdot\}^{\mathrm{T}}$ denotes transpose of a vector. The matrix $\mathbf{T}_{1nm}$ consists of the elements of $\mathbf{R}_{nm}$ suitably multiplied by $\mathrm{e}^{-\mathrm{j}k_{inm}L}$, $i = 1, \ldots, 4$, which physically is the matrix of coordinate transformation between the generalized coordinate and the physical coordinate system.

The elements are essentially edge elements and tractions are specified at node 1 and node 2, as shown in Fig. 2. The tractions are balanced by the internal stresses at the surfaces by Cauchey's principle which states, $\{\mathbf{t}\} = [\boldsymbol{\sigma}]\{\mathbf{n}\}$, $\mathbf{t}$ is the vector of surface tractions, $[\boldsymbol{\sigma}]$ is the Cauchey's stress matrix and $\{\mathbf{n}\}$ is the vector of surface normals. As the edge 1 and 2 are normal to the Z axis, the surface normals at node 1 and 2 are given as $\{0, \mp 1\}$, respectively, which in turn states that, at node 1, traction in the direction of X, t_x, is

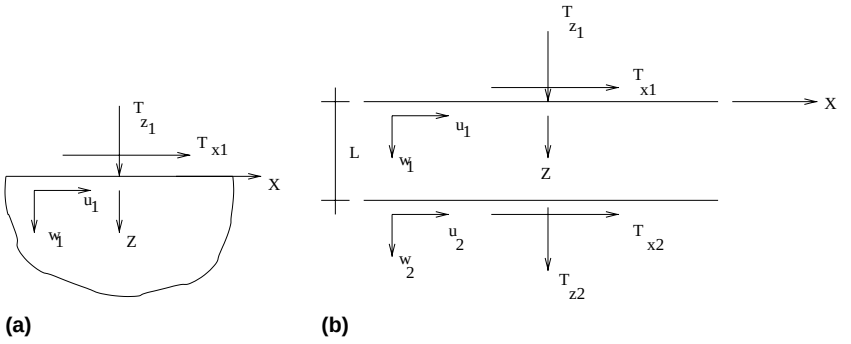

Fig. 2. Sign conventions of (a) throw-off spectral element and (b) layer element.

$-\sigma_{xz}$ and traction in the direction of Z, t_z, is $-\sigma_{zz}$ and at node 2, $t_x = \sigma_{xz}$ and $t_z = \sigma_{zz}$. Relation between the normal stress σ_{zz} and shear stress σ_{xz} to the strains, and in turn, to the displacements can be established by substituting Eq. (2) in Eq. (3), which yields

$$\sigma_{xx} = Q_{11}u_x + Q_{13}w_z, \quad \sigma_{zz} = Q_{13}u_x + Q_{33}w_z, \quad \sigma_{xz} = Q_{55}(u_z + w_x), \tag{22}$$

Substituting Eqs. (15) and (16) in Eq. (22), the stresses can be related to the unknown constants C_i. If the traction–stress relation is utilized and the tractions are evaluated at node 1 and node 2, then a relation is established between tractions at node 1 and 2, $\hat{\mathbf{t}} = \{t_{x1}, t_{z1}, t_{x2}, t_{z2}\}$ and the unknown constants $\mathbf{C}$, as

$$\{\hat{\mathbf{t}}\}_{nm} = [\mathbf{T_2}]_{nm}\{\mathbf{C}\}_{nm}. \tag{23}$$

Explicit forms of $\mathbf{T_2}_{nm}$ and $\mathbf{T_1}_{nm}$ are given in Appendix A (Eqs. (A.1) and (A.2), respectively). Using Eqs. (21) and (23), nodal traction $\hat{\mathbf{t}}_{nm}$ can be related to the nodal displacement $\hat{\mathbf{u}}_{nm}$ as

$$\{\hat{\mathbf{t}}\}_{nm} = [\mathbf{T_2}]_{nm}[\mathbf{T_1}]^{-1}_{nm}\{\hat{\mathbf{u}}\} = [\hat{\mathbf{K}}]_{nm}\{\hat{\mathbf{u}}\}_{nm}, \tag{24}$$

where $\hat{\mathbf{K}}_{nm}$ is the (4×4) element stiffness matrix for ω_n and η_m. It is important to note that, this matrix represents the dynamics of a whole layer of any length L at frequency ω_n and horizontal wavenumber η_m. Consequently, this small matrix of size 4×4, acts as a substitute of the global stiffness matrix of FE modeling, which in general, will be of much larger size, depending upon the thickness of the layer.

2.2. Infinite Layer Element (ILE)

While formulating the FLE, both forward and backward propagating waves are considered. However, another element can be computed where only the forward propagating waves are considered which means no reflection will come back from the boundary. This element is also called throw-off element (as it acts as a conduit to throw away energy from the system) and is very effective in modeling infinite domain in Z directions. This element is also used to impose absorbing boundary conditions or to introduce maximum damping in the structure. The element has only one edge where displacements are to be measured and tractions are to be specified (see Fig. 2a). The displacement field for this element (at ω_n and η_m) is

$$u_{nm} = R_{11}C_{1nm}e^{-jk_1z} + R_{12}C_{2nm}e^{-jk_2z}, \tag{25}$$

$$w_{nm} = R_{21}C_{1nm}e^{-jk_1z} + R_{22}C_{2nm}e^{-jk_2z}, \tag{26}$$

where it is assumed that k_1 and k_2 are the positive roots of Eq. (12). Following the same procedure as before, displacement at node 1 can be related to the constants $C_i, i = 1, \ldots, 2$ as

$$\{\hat{\mathbf{u}}\}_{nm} = [\mathbf{T_1}]_{nm}\{\mathbf{C}\}_{nm}. \tag{27}$$

Similarly, tractions at node 1 can be related to the constants as

$$\{t_{x1} \quad t_{y1}\}^{\mathrm{T}}_{nm} = [\mathbf{T_2}]_{nm}\{C_{1nm} \quad C_{2nm}\}^{\mathrm{T}}, \quad \text{i.e.,} \ \{\hat{\mathbf{t}}\}_{nm} = [\mathbf{T_2}]_{nm}\{\mathbf{C}\}_{nm}. \tag{28}$$

Explicit forms of the matrix $\mathbf{T_1}$ and $\mathbf{T_2}$ are given in Appendix A (Eq. A.2). The tractions at node 1 can be related to the displacements at node 1 as

$$\{\hat{\mathbf{t}}\}_{nm} = [\mathbf{T_2}]_{nm}[\mathbf{T_1}]^{-1}_{nm}\{\hat{\mathbf{u}}\} = [\hat{\mathbf{K}}]_{nm}\{\hat{\mathbf{u}}\}_{nm}, \tag{29}$$

where $\hat{\mathbf{K}}_{nm}$ is the (2×2) element stiffness matrix.

2.3. Expressions of stresses and strains

From the displacement field (Eqs. (15) and (16)) and strain–displacement relation (Eq. (2)), the matrix of strain–nodal displacement relation and stress–nodal displacement relation can be established as

$$\epsilon = \mathbf{B}\mathbf{T}_\mathbf{1}^{-1}\hat{\mathbf{u}}, \quad \sigma = \mathbf{Q}\mathbf{B}\mathbf{T}_\mathbf{1}^{-1}\hat{\mathbf{u}}, \quad \epsilon = \{\epsilon_{xx}, \epsilon_{zz}, \epsilon_{xz}\}, \quad \sigma = \{\sigma_{xx}, \sigma_{zz}, \sigma_{xz}\}, \tag{30}$$

where the elements of $\mathbf{B}$ (size 3×4) are described in terms of the wave amplitude matrix $\mathbf{R}$ and given in Appendix A (Eq. (A.3)). The $\mathbf{Q}$ is the elasticity matrix, which is also given in Appendix A (Eq. (A.4)).

2.4. Prescription of boundary conditions

Essential boundary conditions are prescribed in the usual way as is done in FE methods, where simply the nodal displacements are arrested or released depending the nature of the boundary conditions. The applied tractions are to be prescribed at the nodes. It is assumed that the loading function (for symmetric loading) can be written as

$$F(x,z,t) = \delta(z - z_j)\left(\sum_{m=1}^{M} a_m \cos(\eta_m x)\right)\left(\sum_{n=0}^{N-1} \hat{f}_n \mathrm{e}^{(\mathrm{j}\omega_n t)}\right), \tag{31}$$

where δ denotes the Dirac delta function, z_j is the Z coordinate of the point where load is applied and the z dependency is fixed by suitably choosing the node where the load is prescribed. No variation of load along Z direction is allowed in this analysis. $\hat{f}_n$ are the fourier transform coefficients of the time dependent part of the load which are computed by FFT and a_m are the fourier series coefficients of the x dependent part of the load.

There are two summations involved in the solution and two associated windows, one in time T and one in space L_x. The discrete frequencies ω_n and discrete horizontal wavenumber η_m are related to these windows by the number of data N and M chosen in each summation, i.e.,

$$\omega_n = 2n\pi/T = 2n\pi/(N\Delta t), \quad \eta_m = 2(m-1)\pi/L_x = 2(m-1)\pi/(M\Delta x), \tag{32}$$

where Δt and Δx are the temporal and spatial sample rate, respectively.

2.5. Propagation of Lamb waves

As defined earlier, Lamb waves are guided waves (see Fig. 3(a)), propagating in a free plate and the two lateral guiding surfaces are traction free. There are two main approaches to the analysis of the Lamb waves. The first one is the method of potentials. In this method, Helmhöltz decomposition of the displacement field is obtained and the governing equations are uncoupled and written in terms of the potentials. Solutions are sought for these potentials, which contains four arbitrary constants. The displacement field and the stresses

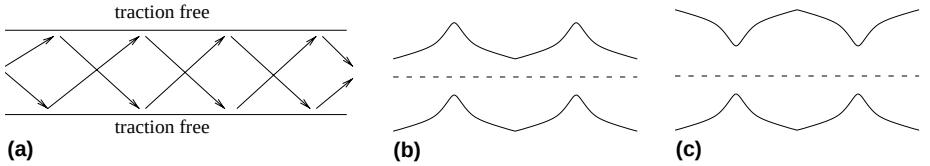

Fig. 3. Propagation and modes of Lamb wave: (a) propagation of Lamb waves, (b) anti-symmetric mode and (c) symmetric mode.

are expressed in terms of the potentials and the imposition of the tractions free upper and lower surfaces generates the necessary condition for finding the unknown constants and the dispersion equation, (see Rose, 1999). The advantage of this method is that the symmetric and anti-symmetric modes can be isolated during formulation, (see Fig. 3(b) and (c)).

The second approach is the partial wave technique, which is discussed below in detail. In the SLE formulation, there are two summations in the solutions. The outer one is over discrete frequencies and the inner one is over discrete horizontal wavenumbers. Each partial wave of Eq. (19) satisfies the governing PDEs (Eq. (4)) and the coefficients C_i as a whole satisfy any prescribed boundary conditions. As long as the prescribed natural boundary conditions are non-homogeneous, no restriction upon the horizontal wavenumber η is imposed and that leads to double summation solution of the displacement field. However, that is not the case for traction free boundary conditions on the two surfaces, which are the necessary condition for generating Lamb waves. The governing discrete equation for finite layer (Eq. (24)) in this case becomes

$$[\hat{\mathbf{K}}(\eta_m, \omega_n)]_{nm}\{\hat{\mathbf{u}}\}_{nm} = 0, \tag{33}$$

and we are interested in a non-trivial $\mathbf{u}$. Hence, the stiffness matrix $\hat{\mathbf{K}}$ must be singular, i.e., $\det(\hat{\mathbf{K}}(\eta_m, \omega_n)) = 0$, which is the required relation between η_m and ω_n. Since, ω_n is made to vary independently, above relation must be solved for η_m to render the stiffness matrix singular, i.e., η_m cannot vary independently. More precisely, for each value of ω_n there is a set of values of horizontal wavenumber η_m (one for each mode) and for each value of ω_n and η_m there are four vertical wavenumbers k_{nm}. The difference in this case is in the value of η_m, which is to be solved for, as opposed to its expression in Eq. (32) and M is the number of Lamb modes considered rather than Fourier modes. Now, for each set of $(\omega_n, \eta_m, k_{nml}), l = 1, \ldots, 4$, $\hat{\mathbf{K}}$ will be singular and $C_l, l = 1, \ldots, 4$ will be in the null space of $\hat{\mathbf{K}}$. Now using Eq. (19), total solution can be constructed. Following the normal practice, the traction free boundary conditions are prescribed at $z = \mp h/2$. Using Eq. (30), the governing equation for C_i and η_m becomes

$$[\mathbf{W}_2(\eta_m, \omega_n)]\{\mathbf{C}\}_{nm} = \mathbf{0}, \quad \mathbf{C} = \{C_1, C_2, C_3, C_4\}, \tag{34}$$

where $\mathbf{W}_2$ is another form of the stiffness matrix $\mathbf{K}$ and is given in Appendix A. The dispersion relation is $\det\{\mathbf{W}_2\} = 0$, which will yield $\eta_m(\omega_n)$ and the phase speed for Lamb waves c_{nm} will be given by ω_n/η_m. Once the values of η_m are known for the desired number of modes, the elements of $\mathbf{C}_{nm}$ are obtained by the technique of SVD as described earlier to find the elements of $\mathbf{R}$. Summing over all the Lamb modes, the solution for each frequency is obtained.

3. Numerical examples

The developed spectral element is validated first to establish its accuracy and efficiency with respect to conventional 2D FE solutions. Next, stress wave propagation through layered anisotropic media is studied. Subsequently, propagation of Lamb waves through layered media is studied. Finally, the present

formulation is utilized to show its advantage in solving inverse problems such as force identification from the measured response.

3.1. Verification of the SLE

Wave propagation in asymmetrically stacked composite layer is studied in this section and the results are compared with 2D FE solutions. The material taken is GFRP composites, which has following material properties: $E_1 = 144.48$ GPa, $E_3 = 9.63$ GPa, $G_{13} = 4.13$ GPa, $v_{13} = 0.3$, $v_{12} = 0.02$ and $\rho = 1389$ kg/m^3. The ply-sequence considered is $[0°_{10}/90°_{10}/0°_{10}]$, where each laminae is 0.01 m thick. This large thickness is chosen to differentiate between incident and reflected pulse, although any layer thickness can be chosen. The layered system is impacted by a high frequency loading, as shown in Fig. 4. The time history of the load along with its spectrum is shown in Fig. 5. As is seen there, the load is of unit magnitude and 50 μs duration with an initial padding of 100 μs. The load has high frequency content (around 46 kHz). This kind of high frequency load excites many natural modes and the resulting response is suitable linear combination of all these modes. Mode superposition method of analysis for this kind of loading will be computationally too expensive and that is where the present element and formulation are most useful.

The load is applied at the centre of the top layer first in Z direction, which generates primarily QP wave and then in X direction, which generates primarily QSV wave. Response of the structure is measured at several locations along the surface and interfaces. For FE analysis, the layer is modeled with 3600, 3 noded plane-strain FEs. In comparison, there are only 3 FLEs in the spectral model. The FE model results a global system matrix of size 3656×126, whereas, the spectral model results a global system matrix (dynamic stiffness matrix) of size 6×6. While solving via FE analysis, Newmark time integration is adopted with a time increment of 1 μs which means, to get a time history up to 600 μs, the global matrix need to be back-substituted 600 times. For the spectral analysis, the load is sampled at 48.83 Hz with 2048 (N in Eq. (31)) FFT points. Further, for spatial variation, 32 fourier series coefficients (M in Eq. (31)) are considered. For concentrated load all the a_ms are equal to $2/X_L$, where X_L is the window length in X direction, here taken as 1.0 m, as per the FE model. Since, the time domain response is real, the computation of displacements (or velocities) needs to be carried out only up to the Nyquist frequency. Hence, the global stiffness matrix need to be inverted 1025×32 times. This computational requirement is many order smaller compared to the requirement of the FE analysis. Further, a typical simulation in FE takes 110 s of CPU time, whereas, a SE run takes 14 s in Compaq Alpha Server ES40 with DEC compiler.

Before discussing the velocity histories (and subsequently plotted stress histories) few points need to considered. When a velocity wave encounters a stiffer zone the reflected wave has equal magnitude with opposite sign of the incident wave. As opposed to that, when the wave encounters a zone of comparatively lower stiffness, the reflected wave has equal amplitude with same sign of the incident wave. These

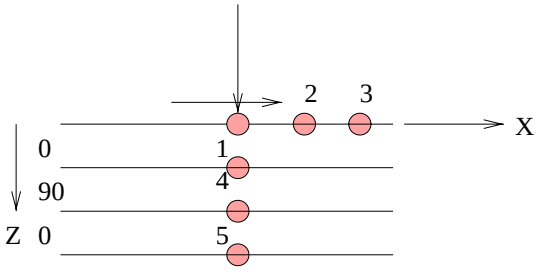

Fig. 4. Layer model for verification.

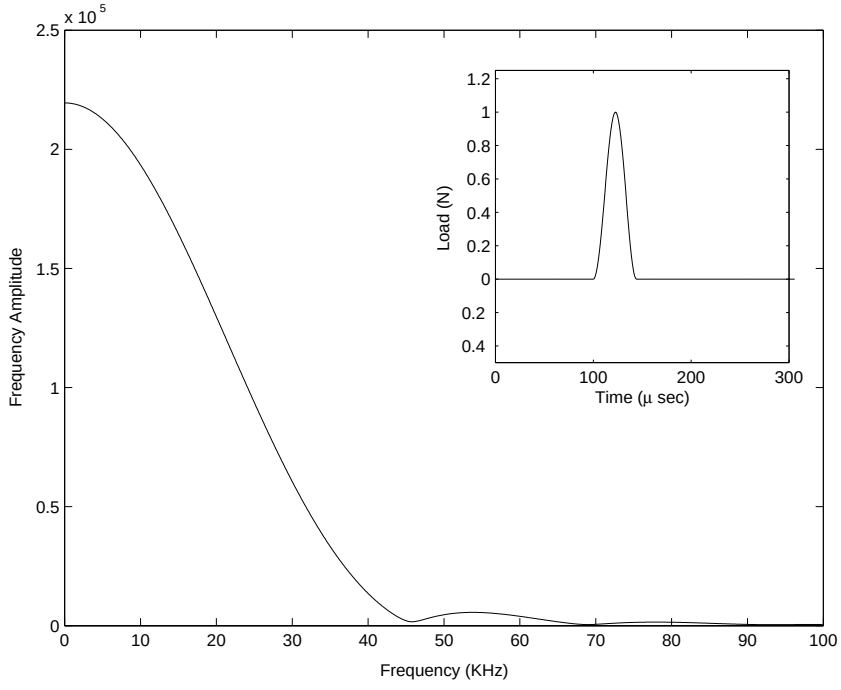

Fig. 5. Load applied for verification study.

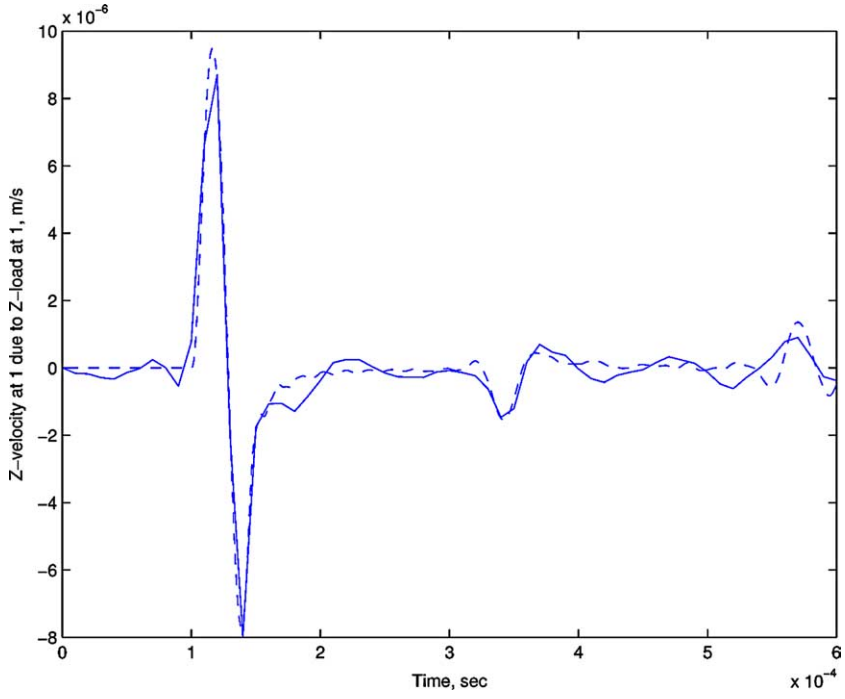

Fig. 6. QP wave at the surface (point 1), solid line—SE, dashed line—2D FE.

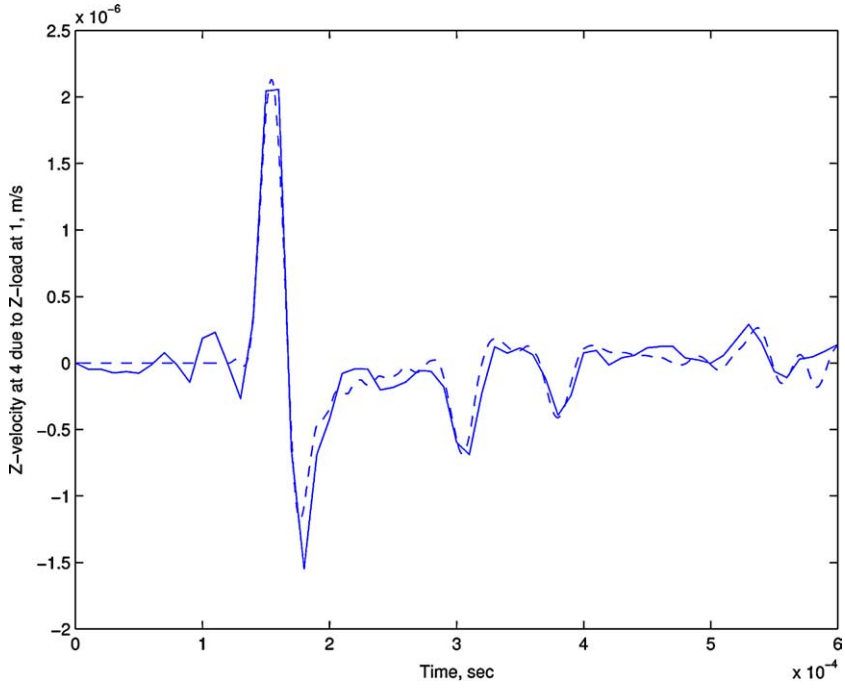

Fig. 7. QP wave at the interface, solid line—SE, dashed line—2D FE.

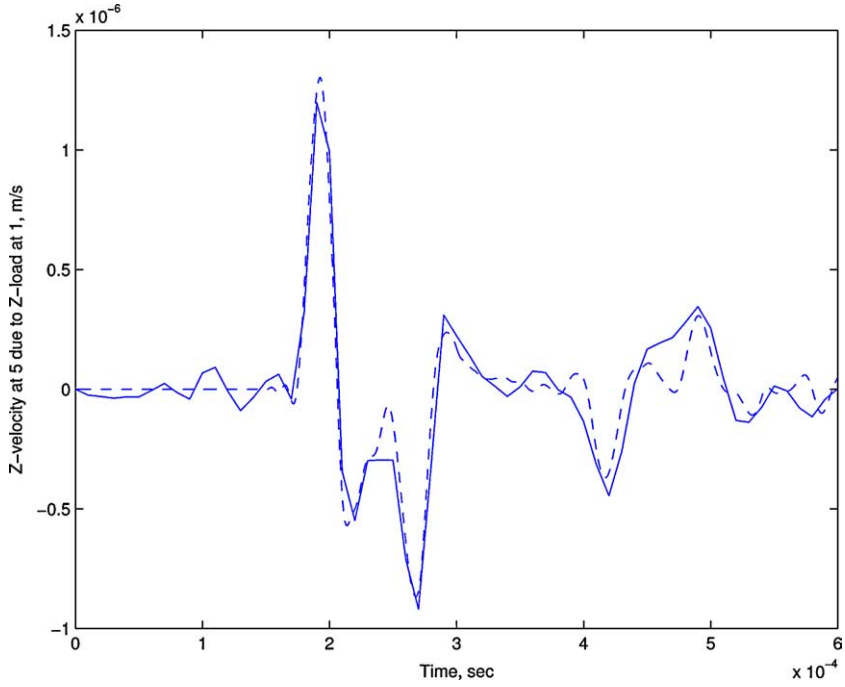

Fig. 8. QP wave at the interface, solid line—SE, dashed line—2D FE.

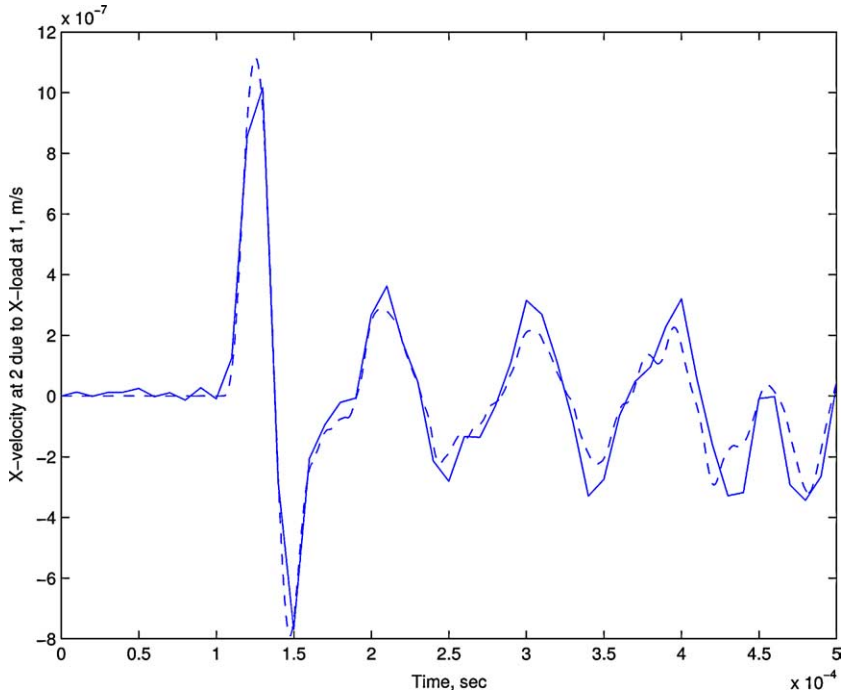

Fig. 9. QSV wave at the surface, solid line—SE, dashed line—2D FE.

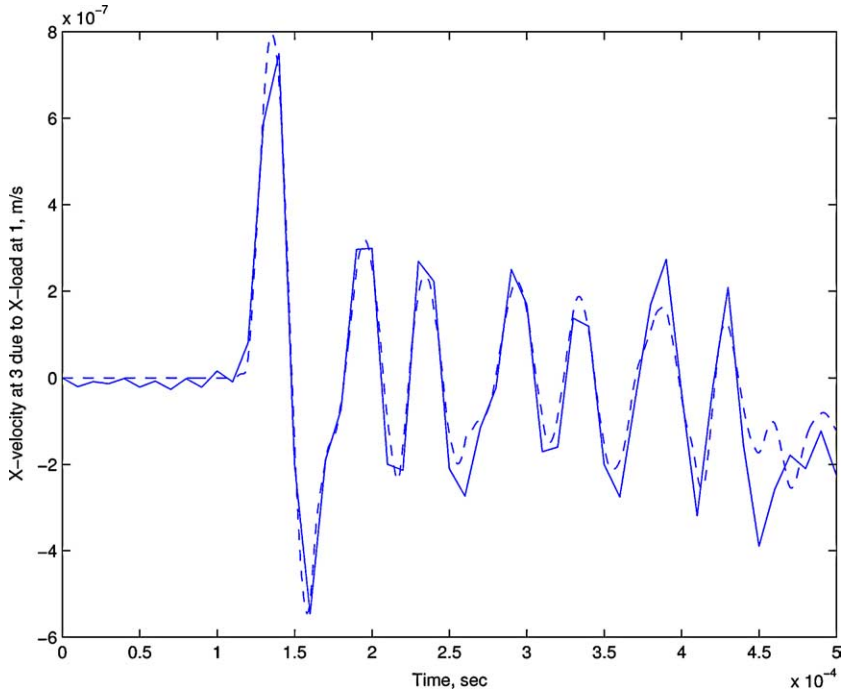

Fig. 10. QSV wave at the surface, solid line—SE, dashed line—2D FE.

phenomena are best visible in the reflections from the fixed end (infinite stiffness) and free end (zero stiffness) of a structure. However, reflected waves are also generated at the interfaces of laminates because of mismatch in stiffness and hence in impedance. In the present model, propagation is considered in the direction of ply-stacking and there is nominal change in stiffness in that direction, due to change in laminae angle. Hence, the magnitude of the reflected waves from the interface will not be large enough to be visible, in comparison to the boundary generated waves. Thus whatever reflections are present in the velocity or stress history are solely due to reflections from the boundary.

For the load applied in Z direction at point 1, Z directional velocity $\dot{w}$, is measured at points marked by 1, 4, and 5. The velocity history of these nodes are plotted in Figs. 6–8. In Fig. 6, peak at 100 μs is the direct effect of the load. For this kind of loading the propagating wave is essentially QP wave. In this case, the inverted peak at around 3.2×10^{-4} s is the reflection from the fixed end, i.e., at $z = 0.3$ m. Again at the fixed end, the wave gets inverted and shows up at around 5.4×10^{-4} s. This figure also shows the excellent agreement between the FE and SLE responses.

Next, the $\dot{w}$ history at first interface ($z = 0.1$ m, point marked by 4) is plotted in Fig. 7. The response in this case does not start at 100 μs as before, but at 130 μs. This time is taken for propagation in the first layer, i.e., 0° laminate. Subsequent reflections at around 2.9×10^{-4} s and 3.6×10^{-4} s are due to reflections from the fixed edge ($z = 0.3$ m) and free edge ($z = 0.0$ m), respectively. Further, the peak at around 5.0×10^{-4} s is the second reflection from the fixed edge.

For the $\dot{w}$ history measured at second interface ($z = 0.2$ m, point marked by 5) and plotted in Fig. 8 the main peak comes down to 1.67×10^{-4} s because of large travelling distance. The QP wave velocity at 90° laminate is lesser than that in 0° laminate and hence this increase (above 1.6×10^{-4}) in propagation time. There are reflections from the fixed end (inverted peak at around 2.46×10^{-4} s), reflections from the free end (inverted peak at 4.0×10^{-4} s) and the second reflections from the fixed end (peak at around 4.7×10^{-4} s). The SLE captures these reflections quite well and except at the last reflection, the response matches satisfactorily with FE response.

Next, the same load is applied at point 1 in X direction. For this load primarily QSV wave is generated. There will be no wave at the impact point and X directional velocity $\dot{u}$ is measured at the surface points 2 and 3 and plotted in Figs. 9 and 10, respectively. In both the cases several reflections from the fixed ends are visible. As before, good agreement between FE and SLE responses can be observed. These responses establish the developed SLE in terms of accuracy, efficiency and cheap cost of computation.

3.2. Propagation of stress waves in layered media

In this section, the formulated element is employed to study the stress wave propagation in layered media, which is very important from structural health point of view. In particular, inter-laminar normal (σ_{zz}) and shear (σ_{xz}) stresses are of great concern as they are root cause for delamination in composite. The same layered system of previous example is taken in this study. Tractions are specified in both X and Z direction, where the same load history (Fig. 5) is applied. It is to be noted that, for stress wave, fixed end generates a reflected wave of having same magnitude and sign of the incident wave, and free end generates a reflected wave of same magnitude but opposite sign of the incident wave.

First, the traction is applied in Z direction and normal stress σ_{zz} is measured at point 1, 4 and 5. The normalized (with respect to the maximum magnitude in each case) measured stresses are shown in Fig. 11. As is seen there, at the surface the stress history profile is exactly the same as the applied traction, which is expected. However, at the interfaces the initial peak appears after a certain interval of time due to finite propagation speed. Further, multiple reflections are visible at the interfaces, which results both tensile and compressive stresses. These stresses will be responsible for delamination or matrix cracking, if they exceed the allowable limit. For the stress wave measured at the second interface, the first positive peak is the reflection from the fixed end and subsequent negative peak is the reflection from the free end. Similarly, the

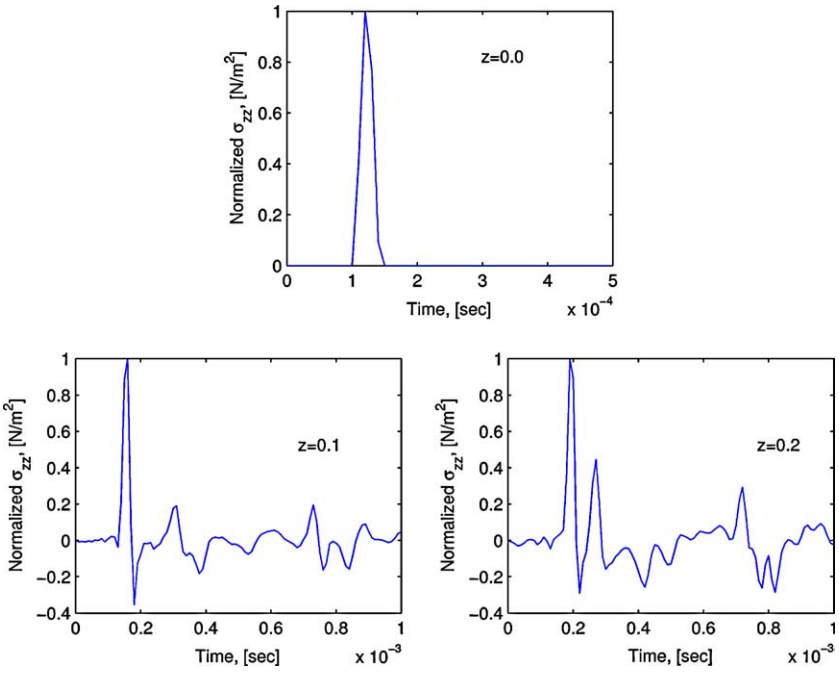

Fig. 11. Stress wave propagation, σ_{zz} due to t_z.

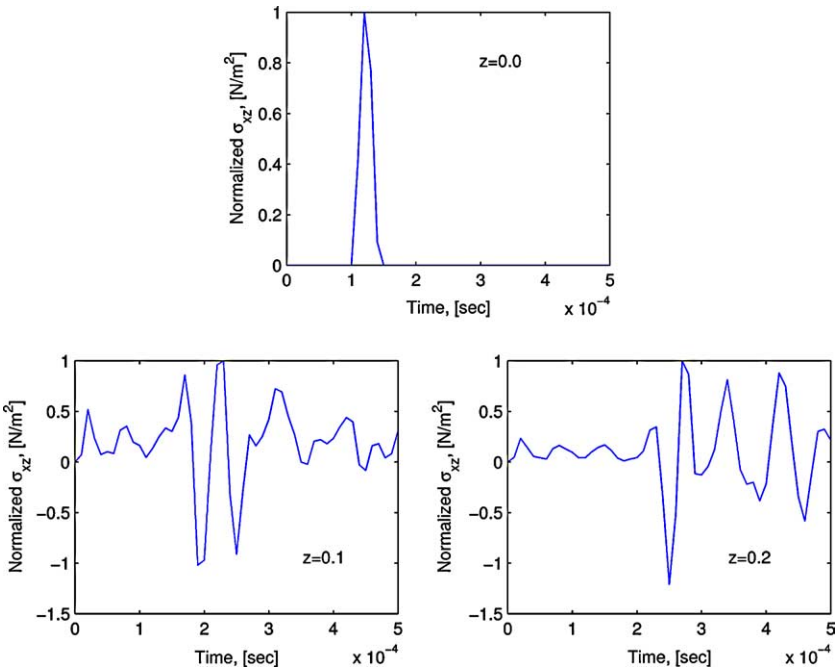

Fig. 12. Stress wave propagation, σ_{xz} due to t_x.

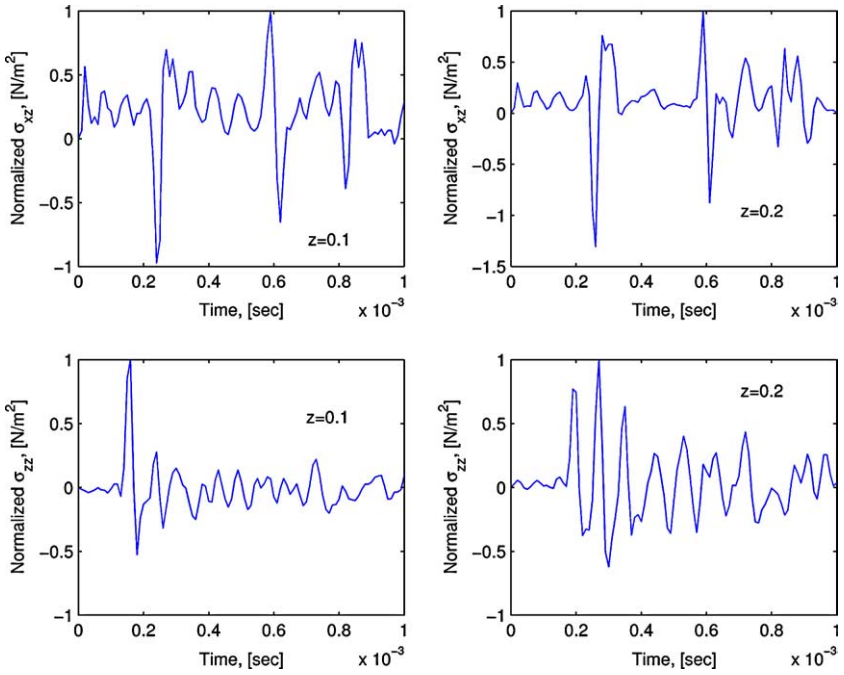

Fig. 13. Stress wave propagation, σ_{xz} due to t_z and σ_{zz} due to t_x.

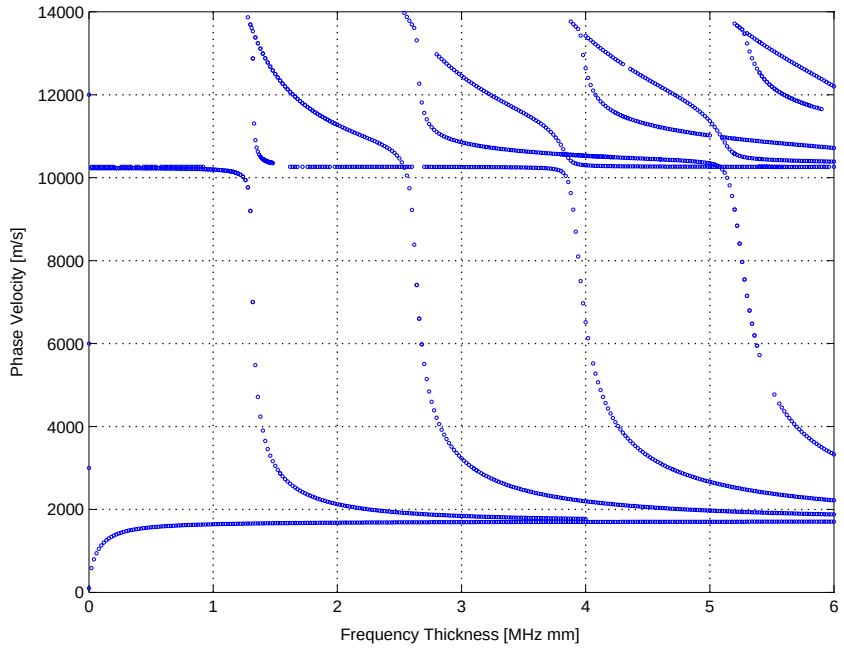

Fig. 14. Lamb wave modes for 0° ply-angle.

second negative peak is the second reflection from the fixed end, whereas, the second positive peak is the second reflection from the free end. Similar traits are visible in the stress wave measured at the second interface ($z = 0.2$ m). The shear stresses generated at the interfaces due to this load is plotted in the top two subplots of Fig. 13. No shear stress is generated at the top surface. Although their magnitude is very less compared to the normal stresses, their existence may prove fatal sometimes. Most importantly, reversal of stresses at the interfaces can cause severe damage to the structure.

Next, the load is applied in X direction and shear stresses at the surface and interfaces are measured at a X coordinate of 0.2 m and plotted in Fig. 12. As usual, the surface stress wave is same as the applied stress, whereas, the main interface wave peaks are of opposite sign. Further, the reflections from the fixed and free ends follow the same trait of the normal stress. The normal stresses generated at the interfaces due to this traction is plotted in the lower two subplots of Fig. 13. Again several reversal of stresses are visible, particularly for the second interface.

Above example shows the general stress pattern that exists in a layered media for applied normal and shear tractions and effect of boundaries on the conversion of these stresses. In particular, boundaries generate stress waves which may be as strong as the original pulse. Further, stress waves can be trapped in a layer, which may cause severe damage in absence of low dissipation rate.

3.3. Propagation of Lamb waves in layered media

A uni-directional laminae of 2 mm. thickness is considered for the study of propagating Lamb wave modes. Analysis is performed for three different fibre-directions are considered, 0°, 45° and 90°. Material

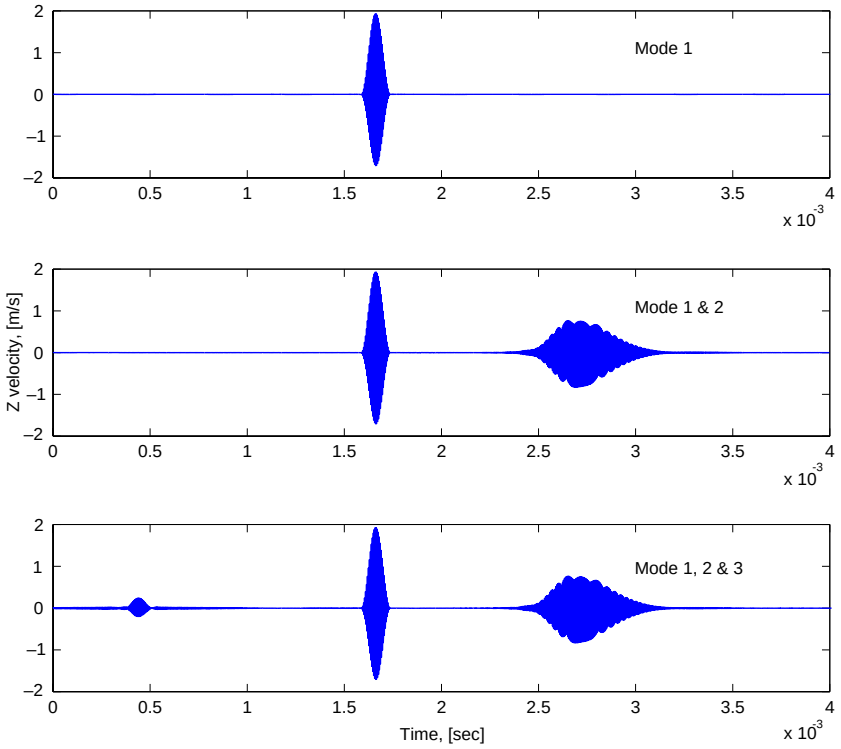

Fig. 15. Lamb wave propagation for 0° ply-angle, $L = 320h$.

properties of the composite are as taken before. The dispersion relation (relation between $c_p = \omega/\eta$ and ω) is usually left in the form of a determinant equal to zero because of its complexity. Hence, solution for this kind of implicit equation requires special treatment. The solution in particular is multi-valued, unbounded and complex (although the real part is of interest). One way to solve these equations is to appeal to the strategies of non-linear optimization, which are based on non-linear least square methods. There are several choices of algorithms, like trust-region dogleg method, Gauss–Newton method with a line search, or a Levenberg–Merquardt method with line-search. Here, MATLAB function *fsolve* is used and the default option for medium scale optimization—the trust-region dogleg method is adopted, which is a variant of the Powell's dogleg method (Powell, 1970).

Apart from the choice of algorithm there are other subtle issues in root capturing for the solution of wavenumbers as the solutions are complicated in nature. Moreover, except the first one or two modes, all the other roots escape to infinity at low frequency. For isotropic materials, these critical frequencies are known below which the phase speed is infinite. However, no expressions can be found for anisotropic materials and most of the times, the modes (solutions) should be tracked backward, i.e., from higher frequency to lower frequency. In general two strategies are essential to capture all the modes within a given frequency band. Initially, the whole region should be swept for different values of the initial guess, where the initial guess should remain constant for the whole range of frequency. These sweeping opens up all the modes in that region, although they are not completely traced. subsequently, each individual mode should be followed to the end of the domain or to a pre-set high value of the solution. For this case, the initial guess should be changed for each frequency to the solution of the previous frequency step. Also, sometimes it is necessary to reduce the frequency step in the vicinity of high gradient of the modes. Once the Lamb modes are generated they are fed back into the frequency loop to generate the frequency domain solution of the Lamb wave propagation, which through IFFT produces the time domain signal. As the Lamb modes are generated first, they need to be stored separately. To this end data are collected from the generated modes at several discrete points in the whole range of frequency. Next, a cubic spline interpolation is performed for a very fine frequency step within the same range. While generating the time domain data, interpolation is performed from these finely graded data to get the phase speed (hence, η).

To get the time history of propagating Lamb waves a modulated pulse of 200 kHz center frequency is applied at one end of an infinite plate and X and Z velocities are measured for a propagating distance of 320h, where h is the thickness of the plate. While studying the time domain representation, the thickness of the plate is taken as 10 mm, which amounts to a frequency-thickness value of 2. This increased thickness is taken because for this value, atleast three modes will be excited in all the cases, as shown by their respective dispersion curves (Figs. 14, 17 and 20). To get the same frequency-thickness value otherwise, we have to increase the frequency content of the load to 750 or 800 kHz, which is computationally prohibitive.

In all the plots of Lamb modes the abscissa is given in terms of frequency times the thickness. Fig. 14 shows the first 10 Lamb modes for fibre angle 0°. As is seen in there, first anti-symmetric mode (Mode 1) converges to a value of 1719 m/s in a range of 1 MHz mm, where all the other modes converge at various later values of frequency. In analogy to the isotropic case, this is the velocity of Rayleigh surface waves in 0° fibre laminae. The first symmetric mode (Mode 2) starts above 10 000 m/s and drops suddenly at around 1.3 MHz mm to converge to 1719 m/s, before which it has fairly constant value. All the other higher order modes escape to infinity at various point in the frequency range. Also the symmetric and anti-symmetric pair of each mode escape almost at the same frequency.

Propagation of these modes are plotted in Figs. 15 and 16 for first three modes (a_0, s_0 and a_1), here referred as Mode 1, 2 and 3 respectively. In Fig. 15, the Z velocity history is plotted, whereas in Fig. 16 the X velocity history is plotted. The figures readily show the different propagating modes, each corresponds to one blob. It is to be noted that, wave propagation velocity is given by the group speed (and

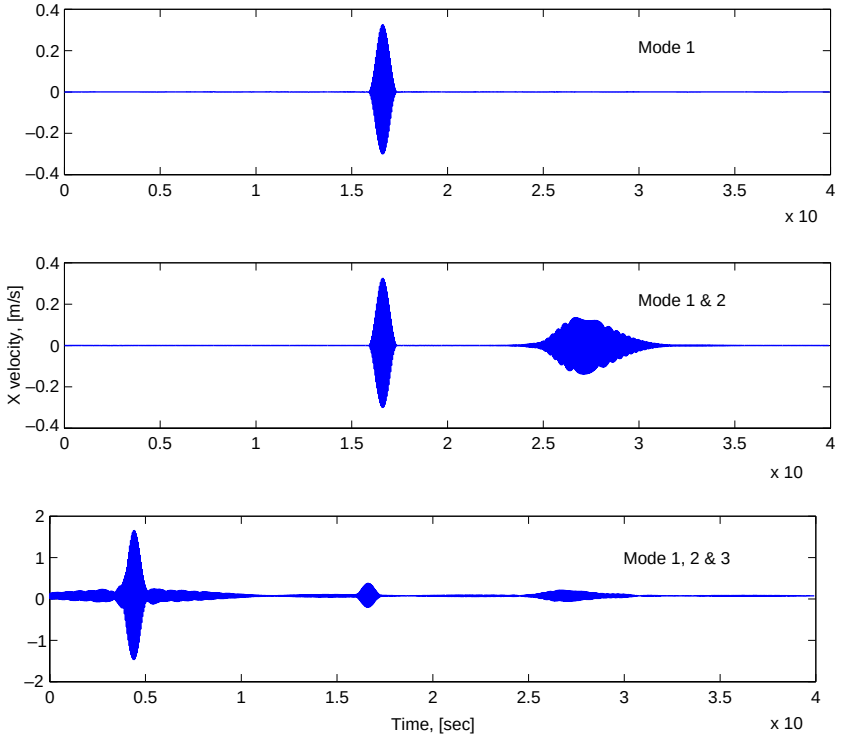

Fig. 16. Lamb wave propagation for 0° ply-angle, $L = 320h$.

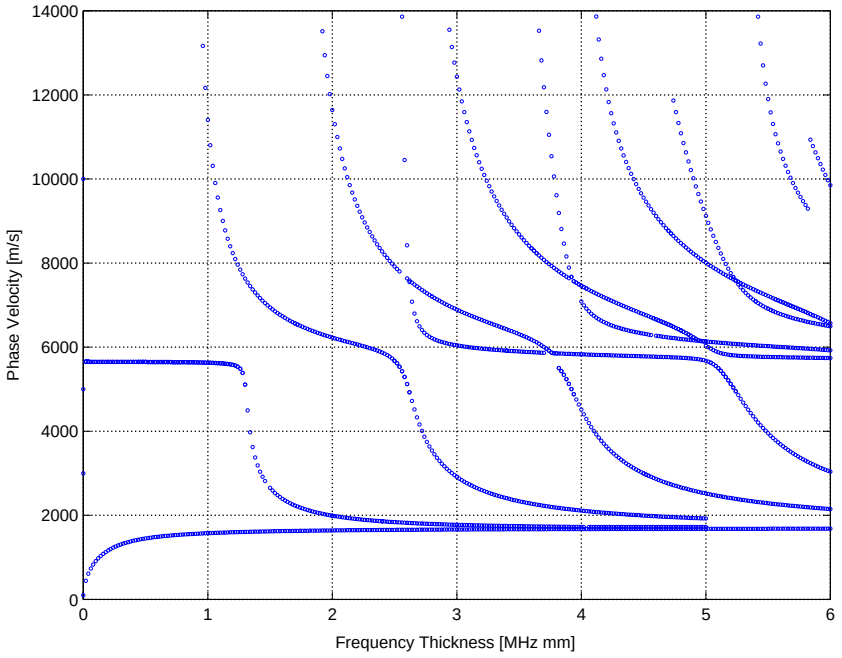

Fig. 17. Lamb wave modes for 45° ply-angle.

not the phase speed). Hence, Fig. 14 will not help us to predict the appearances of different modes. However, as Fig. 15 and 16 suggest, mode 2 has a lower group speed than mode 1 and mode 3 has a group speed much higher than both mode 1 and 2. One difference in the $\dot{u}$ and $\dot{w}$ history can be observed. For $\dot{u}$, the higher mode generates velocity of comparatively lesser magnitude, whereas, for $\dot{w}$, the magnitude is highest.

Next the fibre angle is changed to 45° and the Lamb modes are plotted in Fig. 17. Here, the phase velocity of Mode 1 (a_0) is lower than the previous values for 0° (1690 m/s). Also, initial phase velocity of Mode 2 (s_0) has come down to less than 6000 m/s in comparison to its 0° counterpart (10 000 m/s). Further, critical frequencies of all the higher modes are lower compared to the previous case. Also there are considerable differences in this critical frequencies for each pair of symmetric and anti-symmetric modes, which is absent 0° case. Moreover, number of modes also is increased to 11 from 10 in the previous case. The time domain representation of the propagating waves are shown in Figs. 18 and 19. In this case, however, the second mode has higher group velocity than the first mode and the third mode has the highest group speed.

Finally, the fibre angle is changed to 90° and the resulting mode shapes are plotted in Fig. 20. The shifting of the modes to the left of the figure continues as the number of modes is increased to 12. Further, the first symmetric mode has come down to 2600 m/s and the first anti-symmetric mode is reduced to a converged speed of 1510 m/s. For this modes the propagating Lamb wave is plotted in Fig. 21 and 22 for $\dot{u}$ and $\dot{w}$, respectively. As the figures suggest, mode 2 again has lower group speed compared to mode 1 and mode 3 has higher speed than both mode 1 and 2. However, the difference

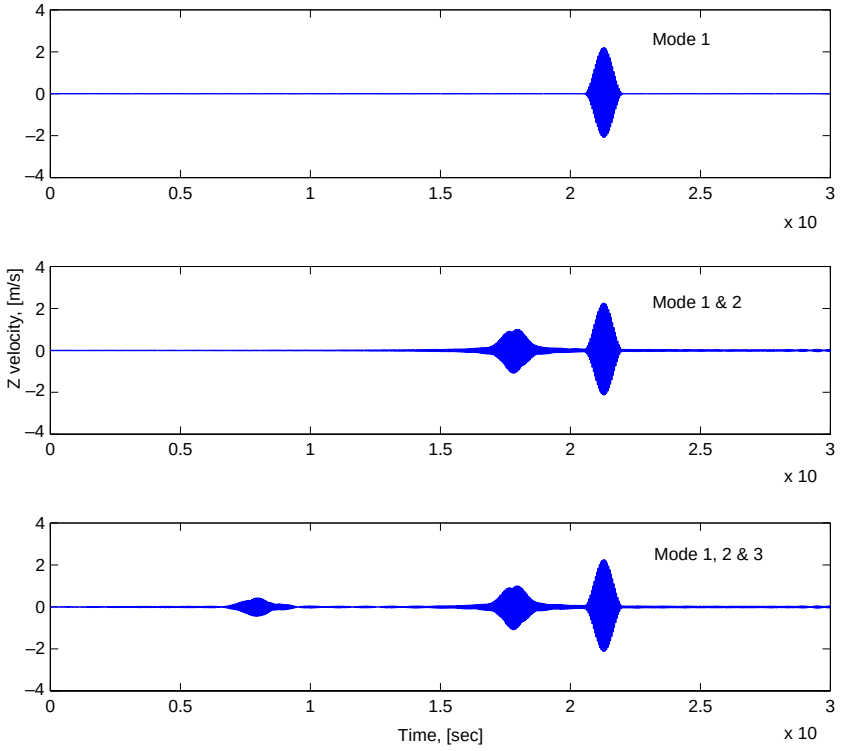

Fig. 18. Lamb wave propagation for 45° ply-angle, $L = 320h$.

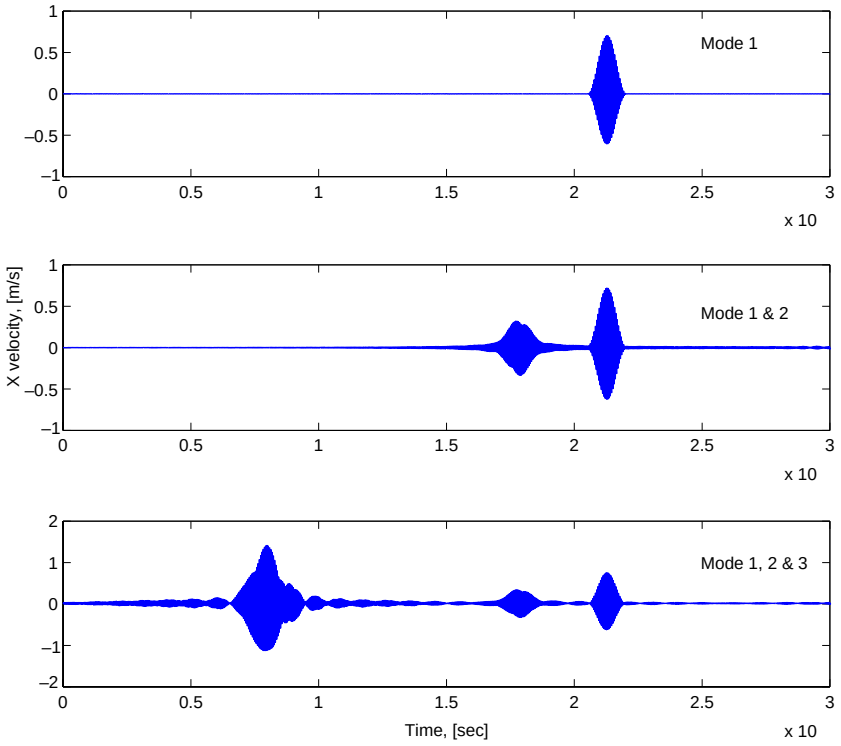

Fig. 19. Lamb wave propagation for 45° ply-angle, $L = 320h$.

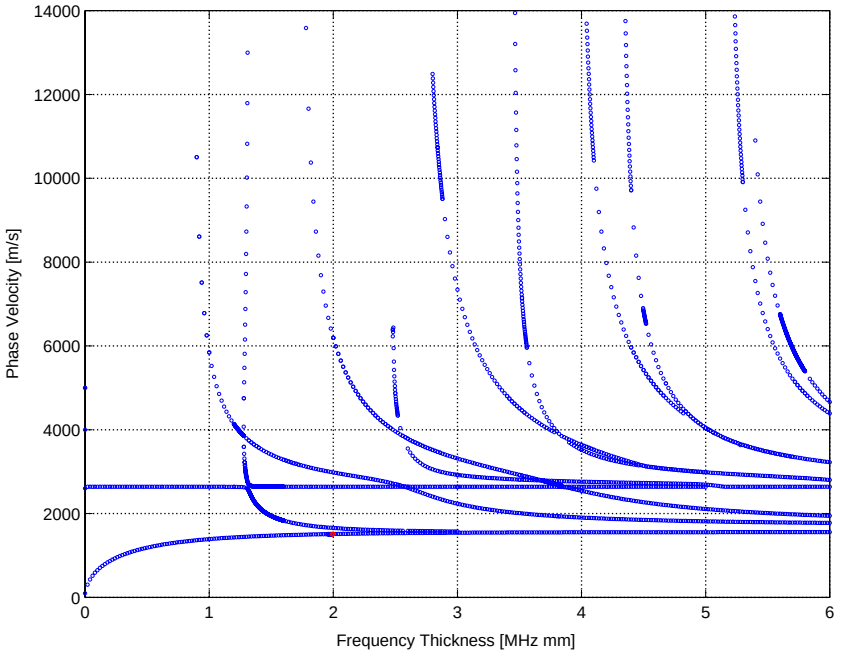

Fig. 20. Lamb wave modes for 90° ply-angle.

between the mode 3 group speed and mode 2 group speed is not very high as opposed to the previous cases.

3.4. Force reconstruction from truncated response

The basic idea of force identification in frequency domain analyze is presented below. Since the whole spectral formulation is in the frequency/wavenumber domain, the response is related to the input through the transfer function in the frequency/wavenumber domain as

$$\tilde{Y}(\omega_n, \eta_m) = \tilde{H}(\omega_n, \eta_m)\tilde{X}(\omega_n, \eta_m), \tag{35}$$

where $\tilde{X}(\omega_n, \eta_m)$ is the transformation of the input (say, load), $\tilde{Y}(\omega_n, \eta_m)$ is the transform of the output (typically, velocity, strain etc.), and $\tilde{H}(\omega_n, \eta_m)$ is the system transfer function. Now, input force can be obtained easily by dividing the transform of the response by the transfer function, that is,

$$\tilde{X}(\omega_n, \eta_m) = \tilde{Y}(\omega_n, \eta_m)/\tilde{H}(\omega_n, \eta_m). \tag{36}$$

Thus, if the response is known at some point, then the disturbance that caused it can be computed. This is one of the distinct advantage of the spectral approach in its ability to solve inverse problems.

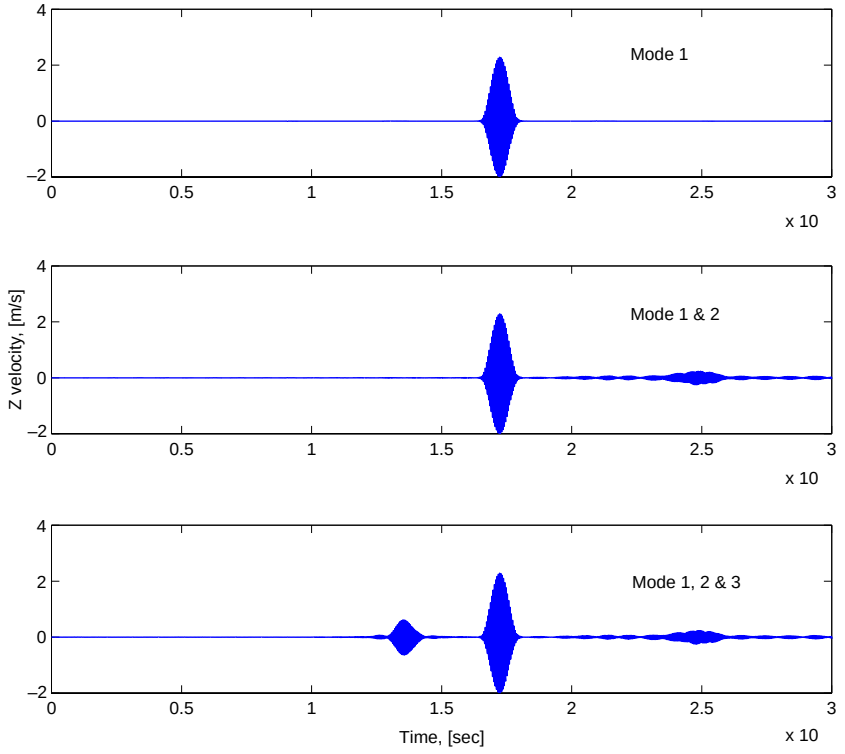

Fig. 21. Lamb wave propagation for 90° ply-angle, $L = 320h$.

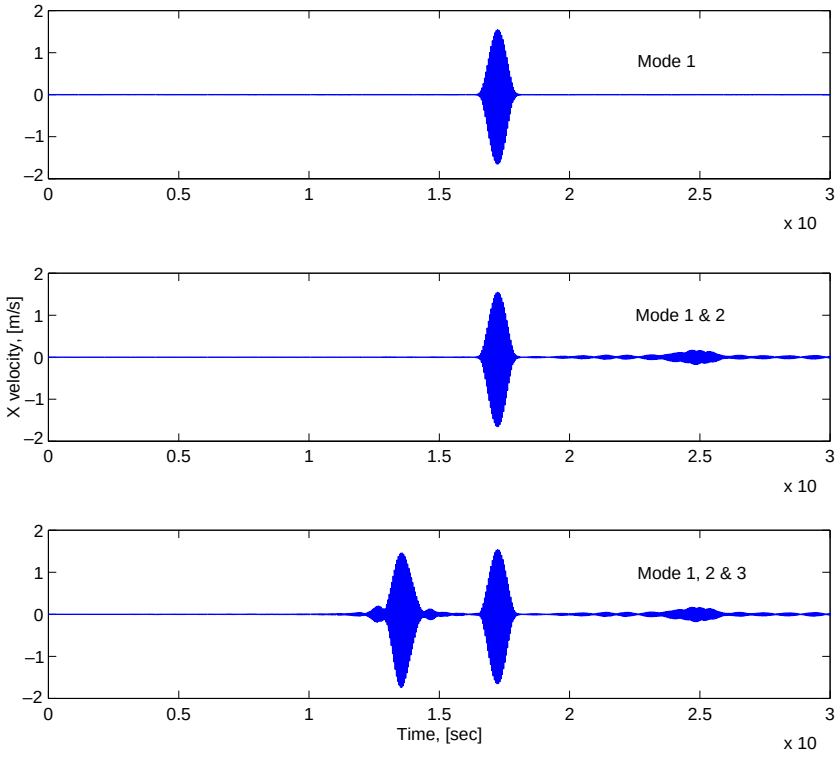

Fig. 22. Lamb wave propagation for 90° ply-angle, $L = 320h$.

In general, $\tilde{Y}(\omega_n, \eta_m)$ will be experimental data, typically transform of strain history (Rizzi, 1989). In this work, FE analysis output is taken as a replacement of experimental output and when this response is fed into the spectral solver the applied force can be reconstructed. The experimental outputs are always truncated at some point. This is the reason why the FE output is also truncated to simulate the experimental output. It is to be noted that, the present model is a second order system, where in most of the cases the waves are non-dispersive in nature. The tracking of reflection is quite simple in such systems.

The layered system of the verification study is taken here and the same load is applied at point 1. The FE signal taken as a substitute for experimental output is the response of Fig. 6, shown in dashed line. This FE signal is truncated at three different times (t_c), 1000, 500 and 250 μs. The truncated responses are shown in Fig. 23. When these responses are given as input in the spectral solver force history comes as output. These histories are plotted in Fig. 24 for the three different cut-off points. As is seen in the figure, for the truncation time of 1000 μs, reconstructed force history matches almost exactly with the original force history. The second and third truncated signals ($t_c = 500$ and 250 μs, respectively) also generate the initial form of the load history quite accurately. However, the second truncated signal registers an inverted peak at around 700 μs and the third signal shows another extra peak at around 350 μs, which are not present in the original history. Surely, these responses arise because of the removal of later part of the FE response. Thus, the peak at 700 μs arise due to removal of second and subsequent reflections from the fixed end and the peak at 350 μs is due to the removal of the first reflection from the fixed end. Hence, if it is known that there is only one impact load and only the

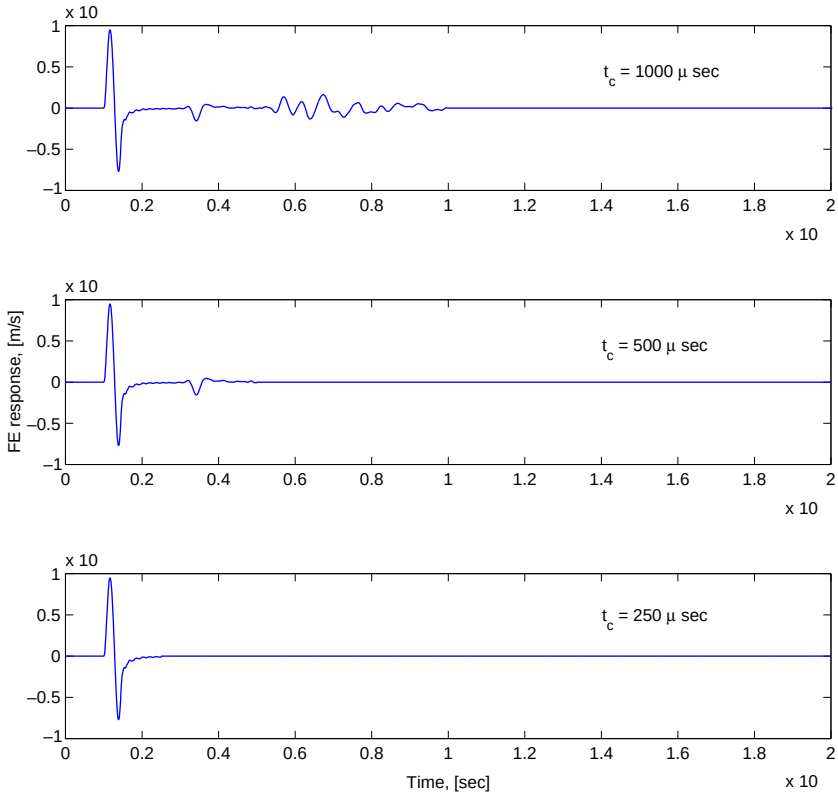

Fig. 23. FE response truncated at several points.

duration and magnitude of that load is desired, FE response (or the experiment output) can be truncated at any point after the main peak. This exercise further demonstrates the inherent efficiency of the spectral formulation in source reconstruction.

4. Conclusion

A spectral element is developed to analyze wave propagation in layered media. The element captures the essential response of layered system to impact loading quite efficiently compared to conventional FE modeling and analysis. Stress state within a multi-layered system reveals trapping of energy and multiple reversal of stresses, which may prove fatal to the safety of the structure. Further, Lamb modes are computed for uni-directional composite laminate and effect of different modes on time domain response is investigated for different fibre angles. It is shown that the increase of ply-angle increases number of active modes within a defined frequency range, reduces escape frequency (frequency where the phase speed becomes infinity) and reduces phase speeds. Finally, inherent advantages of spectral element formulation is utilized to reconstruct applied force history from truncated responses. It has been shown that the later part of the response does not influence the main loading pulse and it is possible to have a fair approximation of the applied pulse from a early truncated signal.

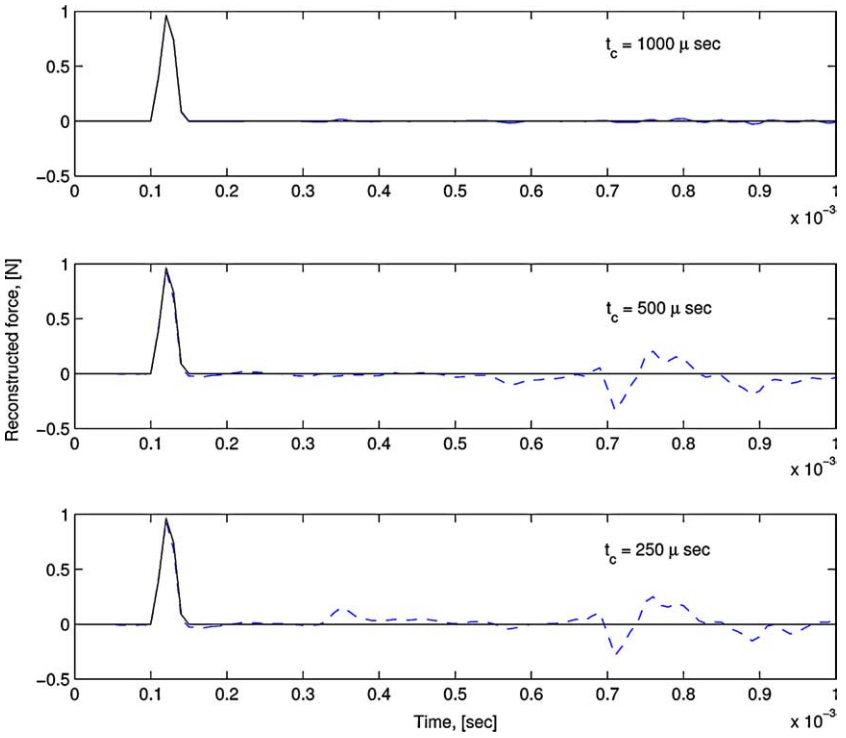

Fig. 24. Reconstructed force history for several truncated responses, solid line—original force history, dashed line—reconstructed force history.

Appendix A

The matrices $\mathbf{T_1}$ and $\mathbf{T_2}$ for the FLE (used in Eqs. (21) and (23)):

$$\mathbf{T_1} = \begin{bmatrix} R_{11} & R_{12} & R_{13} & R_{14} \\ R_{21} & R_{22} & R_{23} & R_{24} \\ R_{11}e^{(-jk_1L)} & R_{12}e^{(-jk_2L)} & R_{13}e^{(+jk_1L)} & R_{14}e^{(+jk_2L)} \\ R_{21}e^{(-jk_1L)} & R_{22}e^{(-jk_2L)} & R_{23}e^{(+jk_1L)} & R_{24}e^{(+jk_2L)} \end{bmatrix}, \tag{A.1}$$

$$T_2(1,p) = -Q_{55}(-jR_{1p}k_p - \eta R_{2p}),$$
$$T_2(2,p) = jQ_{33}R_{2p}k_p - Q_{13}\eta R_{1p},$$
$$T_2(3,p) = Q_{55}(-jR_{1p}k_p - \eta R_{2p})e^{(-jk_pL)}$$
$$T_2(4,p) = \{-jQ_{33}R_{2p}k_p + Q_{13}\eta R_{1p}\}e^{(-jk_pL)},$$

where p ranges from 1 to 4, $k_3 = -k_1$ and $k_4 = -k_2$.

For the ILE, $\mathbf{T_1}$ and $\mathbf{T_2}$ can be obtained by truncating the matrices of FLE. In particular,

$$\mathbf{T_{1(ILE)}} = \mathbf{T_{1(FLE)}}(1:2,1:2), \quad \mathbf{T_{2(ILE)}} = \mathbf{T_{2(FLE)}}(1:2,1:2). \tag{A.2}$$

The matrix of strain–displacement relation, **B** is given by

$$B(1,p) = R_{1p}\eta e^{-jk_p z}, \quad B(2,p) = -jR_{2p}k_p e^{-jk_p z}, \\ B(3,p) = -(jR_{1p}k_p + R_{2p}\eta)e^{-jk_p z}, \tag{A.3}$$

where z is the point of strain measurement. The elasticity matrix **Q** is

$$\mathbf{Q} = \begin{bmatrix} Q_{11} & Q_{13} & 0 \\ Q_{13} & Q_{33} & 0 \\ 0 & 0 & Q_{55} \end{bmatrix}. \tag{A.4}$$

Elements of $\mathbf{W}_2$ (appeared in Eq. (34)) are

$$W_2(1,p) = (Q_{11}R(1,p)\eta - jQ_{13}R(2,p)k_p)e^{jk_p^{h/2}}, \\ W_2(2,p) = (Q_{11}R(1,p)\eta - jQ_{13}R(2,p)k_p)e^{-jk_p^{h/2}}, \\ W_2(3,p) = Q_{55}(-R(1,p)k_p + jR(2,p)\eta)e^{jk_p^{h/2}}, \\ W_2(4,p) = Q_{55}(-R(1,p)k_p + jR(2,p)\eta)e^{-jk_p^{h/2}}.$$

References

Chakraborty, A., Gopalakrishnan, S., 2003. Force identification in a FGM plate using truncated response. In: 44th AIAA/ASME/ASCE/AHS-SDM Conference, Paper No. AIAA 2003-1590, Norfolk, Virginia.

Chakraborty, A., Gopalakrishnan, S., submitted. A new spectral element for the analysis of wave propagation in inhomogeneous layered media. AIAA Journal.

Chatfield, C., 1984. The Analysis of Time Series. Chapman and Hall.

Doyle, J.F., 1984. Further developments in determining the dynamic contact law. Experimental Mechanics 24, 265–270.

Doyle, J.F., 1987a. Determining the contact force during transverse impact of plates. Experimental Mechanics 27, 68–72.

Doyle, J.F., 1987b. Experimentally determining the contact force during the transverse impact of ortho-tropic plates. Journal of Sound and Vibration 118 (3), 441–448.

Doyle, J.F., 1988. A spectrally formulated finite element for longitudinal wave propagation. International Journal of Analytical and Experimental Modal Analysis 3, 1–5.

Doyle, J.F., Farris, T.N., 1990. A spectrally formulated finite element for flexural wave propagation in beams. International Journal of Analytical and Experimental Modal Analysis 5, 13–23.

Doyle, J.F., 1993. Force identification from dynamic response of a bi-material beam. Experimental Mechanics 33, 64–69.

Doyle, J.F., 1997. Wave Propagation in Structures. Springer Verlag.

Gopalakrishnan, S., Martin, M.T., Doyle, J.F., 1992. A matrix methodology for spectral analysis of wave propagation in multiple connected Timoshenko beams. Journal of Sound and Vibration 158 (1), 11–24.

Golub, G., Loan van, C., 1996. Matrix Computation. John Hopkins University Press, Baltimore, Maryland.

Haskell, N.A., 1953. The dispersion of surface waves in multi-layered media. Bulletin of the Seismological Society of America 43, 17–34.

Kennett, B.L.N., 1983. Seismic Wave Propagation in Stratified Media. Cambridge University Press.

Kuhlemeyer, R.L., Lysmer, J., 1973. Finite element accuracy for wave propagation problems. Journal of the Soil Mechanics and Foundations Division, ASCE 99 (SM5), 421–427.

Lih, S.S., Mal, A.K., 1992. Elastodynamic response of a unidirectional composite laminate to concentrated surface loads: Part II. Journal of Applied Mechanics 59, 887–892.

Lih, S.S., Mal, A.K., 1995. On the accuracy of approximate plate theories for wave field calculation in composite laminates. Wave Motion 21, 17–34.

Lih, S.S., Mal, A.K., 1996. Response of multilayered composites to dynamic surface loads. Composites B 29B, 633–641.

Mal, A.K., 2002. Elastic waves from localized sources in composite laminates. International Journal of Solids and Structures 39 (21–22), 5481–5494.

Ma, C.C., Huang, K.C., 1995. Wave propagation in layered elastic media for antiplane deformation. International Journal of Solids and Structures 32 (5), 665–678.

Mal, A.K., Lih, S.S., 1992. Elastodynamic response of a unidirectional composite laminate to concentrated surface loads: Part I. Journal of Applied Mechanics 59, 878–886.

Martin, M.T., Gopalakrishnan, S., Doyle, J.F., 1994. Wave propagation in multiply connected deep waveguides. Journal of Sound and Vibration 174 (4), 521–538.

Moulin, E., Assaad, J., Delebarre, C., Grondel, S., Balageas, D., 2000. Modeling of integrated Lamb waves generation systems using a coupled finite element normal mode expansion method. Ultrasonics 38, 522–526.

Nag, A., Roy Mahapatra, D., Gopalakrishnan, S., Sankar, T.S., 2003. A spectral finite element with embedded delamination for modeling of wave scattering in composite beams. Composites Science and Technology 63 (15), 2187–2200.

Nayfeh, A.H., 1995. Wave Propagation in Layered Anisotropic Media with Application to Composites. North Holland, Amsterdam.

Powell, M.J.D., 1970. A Fortran subroutine for solving systems of nonlinear algebraic equations. In: Rabinowitz, P. (Ed.), Numerical Methods for Nonlinear Algebraic Equations (Chapter 7).

Reddy, J.N., 1996. Mechanics of Laminated Composite Plates. CRC Press.

Rizzi, S.A., 1989. A spectral analysis approach to wave propagation in layered solids. Ph.D. Dissertation, Purdue University.

Rizzi, S.A., Doyle, J.F., 1989. Force identification for impact problem on a half plane. In: Schwer, et al. (Eds.), Computational Techniques for Contact, Impact, Penetration and Perforation of Solids, AMD-Vol. 103. ASME, pp. 163–182.

Rizzi, S.A., Doyle, J.F., 1991. Force identification for impact of a layered system. In: Computational Aspects of Contact, Impact and Penetration. Elmepress International, pp. 222–241.

Rose, J.L., 1999. Ultrasonic Waves in Solid Media. Cambridge University Press.

Roy Mahapatra, D., Gopalakrishnan, S., Shankar, T.S., 2000. Spectral-element-based solution for wave propagation analysis of multiply connected unsymmetric laminated composite beams. Journal of Sound and Vibrations 237 (5), 819–836.

Roy Mahapatra, D., Gopalakrishnan, S., 2003a. A spectral finite element model for analysis of axial–flexural–shear coupled wave propagation in laminated composite beams. Composite Structures 59 (1), 67–88.

Roy Mahapatra, D., Gopalakrishnan, S., 2003b. A spectral finite element for analysis of wave propagation in uniform composite tubes. Journal of Sound and Vibration 268 (3), 429–463.

Solie, L.P., Auld, B.A., 1973. Elastic waves in free anisotropic plates. Journal of the Acoustical Society of America 54, 1.

Thomson, W.T., 1950. Transmission of elastic waves through a stratified media. Journal of Applied Physics 21, 89–93.

Veidt, M., Liub, T., Kitipornchai, S., 2002. Modelling of Lamb waves in composite laminated plates excited by interdigital transducers. NDT & E International 35 (7), 437–447.

Verdict, G.S., Gien, P.H., Burger, C.P., 1996. Finite element study of Lamb wave interactions with holes and through thickness defects in thin metal plates. NDT & E International 29 (4).

Viktorov, I.A., 1967. Rayleigh and Lamb Waves. Plenum Press, NY.

Zhao, G., Rose, J.L., 2003. Boundary element modeling for defect characterization potential in a wave guide. International Journal of Solids and Structures 40 (11), 2645–2658.